T Fluid Dynamics Research
boratory Report No. 63-3

SOME RECENT DEVELOPMENTS IN INTERFERENCE THEORY FOR AERONAUTICAL APPLICATIONS*

by
HOLT ASHLEY

MASSACHUSETTS INSTITUTE OF TECHNOLOGY

JULY 1963

*Supported in part by the U. S. Air Force Office of Scientific Research under Grant AF-AFOSR-156-63 and by Office of Naval Research under Contract NONR-1841 (80).

MIT Fluid Dynamics Research
Laboratory Report No. 63-3

SOME RECENT DEVELOPMENTS IN INTERFERENCE THEORY FOR AERONAUTICAL APPLICATIONS*

by

HOLT ASHLEY**

MASSACHUSETTS INSTITUTE OF TECHNOLOGY

JULY 1963

*This work was supported in part by the U. S. Air Force Office of Scientific Research under Grant AF-AFOSR-156-63 and by Office of Naval Research under Contract NONR-1841 (81). The author is indebted to North American Aviation, Inc., and to Aerospace Division, The Boeing Company, for permission to use certain computed results.

**Department of Aeronautics and Astronautics. This paper is prepared for presentation at the Sixth Symposium of the Division of Fluid Mechanics, Polish Academy of Sciences, Zakopane, September, 1963.

TABLE OF CONTENTS

ABSTRACT

Except for particular examples which have fundamental interest rather than engineering utility, exact solutions to loading problems on three-dimensional lifting surfaces have proved unobtainable even by small-perturbation methods. Beginning with the eminently successful lifting-line idealization, there has resulted a proliferation of theories embodying various physical and consistent or inconsistent mathematical approximations. Nearly all of these are now rendered obsolete by the general availability of digital computation machinery with extraordinary speed and capacity, because the best engineering approach is now unquestionably through numerical treatment of the exact linearized integral equation appropriate to the problem under consideration.

A useful by-product of these developments is that the erstwhile restriction to a single, isolated wing whose mean surface lies close to one coordinate plane no longer need be accepted. Integral representations can be devised for the coupled flow fields due to aggregates of lifting surfaces, combinations of wings and bodies, or nonplanar mean surfaces. A number of applications of this modified approach to the phenomenon known as "interference" are described, some including numerical results and comparisons with experiment. Both steady flight and simple harmonic oscillatory motions of small amplitude are included in the examples. Those flows which involve an incompressible or subsonic main stream are constructed by superposition of properly-oriented doublets of acceleration potential; the singular behavior of the integrals is handled in the same manner as for a planar surface. In supersonic cases the technique adopted consists of an extension of the concept of velocity potential aerodynamic influence coefficients. Specialization to sonic flight speed is discussed, but here the linearization is permissible only when the motion is unsteady.

The paper concludes with a review of related subjects, such as the importance of coupling with flow produced by wing thickness, the influence of a ground-plane, and approximate means of accounting for second-order nonlinearity in supersonic flight.

I. Introduction

Although typical flight vehicles consist of aggregates of adjacent or intersecting lifting surfaces and bodies, classical wing theory has dealt very largely with the airflow around individual, almost-plane configurations in uniform motion. As a consequence, there have been developed various approximate schemes for piecing together the classical solutions — methods that fall under the heading of interference or interaction theory. With the vehicle's motion known, the loading on each element of the interfering system is initially estimated as if all other disturbance sources were removed from the field. Two types of correction are then applied. First, the upwash pattern is computed at each lifting surface which would be generated in its absence by other elements of the system; applying this as an incremental angle of attack, the additional loads are calculated by suitable linearized theory. Second, the upwash due to other elements is found along the centerline of each body. Applying this as an incremental angle-of-attack distribution to the body, loads are found, usually by some modification of the well-known slender body theory. In steady-state interference analysis, both of the foregoing steps can be somewhat refined by extending any large, central body to infinity and working at the Trefftz plane.

An excellent summary of prior literature and of interference procedures along the lines just described will be found in Ferrari's article (Ref. 1). Another useful review of both subsonic and supersonic theory has been published by Lawrence and Flax (Ref. 2). The slender-body approach forms the basis of many contributions, notably Refs. 3, 4, 5, 6 and 7.

Because of its author's interest in dynamic loading and aeroelastic stability, the present paper is especially devoted to streamlined interfering systems performing small simple harmonic oscillations. Steady motion is then included as a low-frequency limit. The literature on such time-dependent flows over multiple surfaces and wing-body combinations is surprisingly sparse. An approximate study of the case of incompressible fluid appears in Ref. 8, pp. 63-75. Statler and Easterbrook (Refs. (9-10) have proposed methods for subsonic flight,

and more recent second-order transonic and supersonic theories for slender midwing-body combinations are described by Landahl (Ref. 11) and others (e.g., Refs. 12). Rodden and Revell (Ref. 23) have also discussed certain interference problems.

Except for particular examples, such as supersonic conical flow and the slender-body limit, exact three-dimensional solutions have proved unobtainable even for planar lifting surfaces in steady flight. This deficiency has led, over the years, to the emergence of numerous analyses embodying various physical and consistent or inconsistent mathematical approximations, which are detailed in the cited references and in several excellent books now available on aeronautical aerodynamics. In this connection, the present paper hopes to emphasize two points. First, the bulk of these approximate methods have been rendered obsolete, save for rough preliminary estimation, by the wide availability of digital computation machinery with extraordinary speed and capacity. Second, the restriction to an isolated, planar wing no longer need be accepted, because systematic integral representations can be devised for the coupled flow fields due to very general interfering systems. Of these observations the former is not particularly original, but the latter has not received the recognition which perhaps it deserves. All of the discussion and numerical applications that follow are designed to illustrate how coupled-flow problems are set up and solved. It is hoped that the examples will be adequate to demonstrate the feasibility of practical realization.

The general framework for constructing mathematical statements is by superposition of doublet and source-type singular solutions of the appropriate differential equations for small perturbations upon a uniform stream U parallel to the positive x-direction. Except for occasional comments about nonlinearities, therefore, linearized ideal-fluid theory is employed throughout. In view of numerous excellent published treatments (e.g. Chapter 1 of Miles, Ref. 7), it hardly seems necessary to give extensive details of the problem setup.

The basic dependent variables are the acceleration or pressure potential

$$\psi(x, y, z, t) \equiv \frac{p_\infty - p}{\rho_\infty} \qquad (1)$$

and the disturbance potential $\varphi(x, y, z, t)$, defined by stating that the total velocity potential of the flow is

$$\Phi \equiv Ux + \varphi \tag{2}$$

Here p is static pressure, ρ is density, and subscript ∞ identifies properties of the remote stream. In terms of Cartesian coordinates x, y, z (Fig. 1) and time t, either φ or ψ is a solution of

$$\nabla^2\varphi - M^2\varphi_{xx} - 2\frac{M}{U}\varphi_{xt} - \frac{M^2}{U^2}\varphi_{tt} = 0, \tag{3}$$

M being the free-stream Mach number. The normal derivative of φ is specified over all wing and body surfaces, the former being replaceable by the two sides of the wing's mean surface. Physical variables must be continuous external to the flight vehicle and its wake, and disturbances must die out appropriately at large distances. The uniqueness of solutions usually has to be assured by invoking an auxiliary condition, such as the Kutta hypothesis of smooth flow-off (continuous ψ or $\nabla\varphi$) at all subsonic trailing edges.

The information of practical interest, once the problem is solved, usually consists of the pressure distribution over all wing and body surfaces or some weighted integral thereof, although occasionally other characteristics of the field are required. Pressure can be obtained from ψ through Eq. (1) or from φ, in most cases, through the linearized Bernoulli equation

$$\frac{p - p_\infty}{\frac{\rho_\infty}{2}U^2} = -\frac{2\varphi_x}{U} - \frac{2\varphi_t}{U^2} \tag{4}$$

In steady flow the dependence on t disappears. When the perturbations are simple harmonic, all dependent variables are replaced with their complex amplitudes (...) by operations such as (R.P. $\equiv$ "Real Part")

$$\varphi(x, y, z, t) = \text{R. P.}\left\{ \bar{\varphi}(x, y, z,) e^{i\omega t} \right\} \tag{5}$$

Also $i\omega$ is substituted for $\partial/\partial t$. The circular frequency ω provides a measure of "unsteadiness" in a given problem when converted to a reduced frequency

$$k \equiv \frac{\omega l}{U}, \tag{6}$$

l being a representative streamwise dimension such as wing semichord or body length.

II. Nonplanar Wings in Subsonic Flight

Consider small-amplitude vibrations of a lifting surface S like the one illustrated in Fig. 1, letting the free surface recede to infinity for the moment. In the examples it is assumed that S has zero thickness. In fact, when S happens to be almost plane, thickness effects may be treated separately and independently from those of angle of attack, camber, etc. The same decoupling can be accomplished in the unsteady loads problem even for nonplanar wings. But it is not generally possible in steady flow, and non-zero thickness must be represented by distributing sources over S, which interact with the doublets describing the lifting part of the field. The procedure is straightforward and adds nothing essential to the present discussion.

Superimposed on the mean-surface shape $z_0(y)$ in Fig. 1 is the small displacement

$$\Delta z(x, y, t) = \Delta \bar{z}(x, y)\, e^{i\omega t} \tag{7}$$

the "real part" operation from Eq. (5) being henceforth dropped. This gives rise to a normal displacement

$$\bar{m}(x, y)\, e^{i\omega t} = \Delta \bar{z}(x, y)\, e^{i\omega t} \sec\theta(y) \tag{8}$$

and to a normal velocity of fluid particles in contact with S

$$v_n(x, y, t) = \left[U \frac{\partial \bar{m}}{\partial x} + i\omega \bar{m} \right] e^{i\omega t} \tag{9}$$

v_n must equal the normal derivative φ_n for all points x, y or x, s on S (s being a single-valued curvilinear spanwise coordinate).

For subsonic flow, ψ is chosen as the primary unknown, since pressure discontinuities occur only through S and the disturbance can therefore be represented by normally oriented doublets of ψ over the bounded area of the wing. From the well-known relation between ψ and φ it is easily shown that the principal boundary condition reads

$$e^{-i\frac{\omega x}{U}} \int_{-\infty}^{x} \frac{\partial \bar{\psi}(\lambda, y, z)}{\partial n}\, e^{i\frac{\omega \lambda}{U}}\, d\lambda = U^2 \left[\frac{\partial \bar{m}}{\partial x} + \frac{i\omega \bar{m}}{U} \right], \tag{10}$$

for(x, y, z) on S'

If a layer of Ψ-doublets is distributed over S, classical methods can be used to establish that the layer's strength is locally proportional to the discontinuity of Ψ, or of p. In incompressible flow, for instance, Eq. (3) reduces to Laplace's equation, the doublet singularity is simply a normal derivative of 1/r, and the solution becomes

$$\overline{\Psi}(x,y,z)$$

$$= \frac{1}{4\pi} \iint_S [\overline{\Psi_U} - \overline{\Psi_L}] \frac{\partial}{\partial n_1} \left[\frac{1}{\sqrt{(x-\xi)^2 + (y-\eta)^2 + [z - z_0(\eta)]^2}} \right] d\xi\, d\sigma \qquad (11)$$

$$= \frac{1}{4\pi\rho_\infty} \iint_S [\overline{p_L} - \overline{p_U}] \frac{\partial}{\partial n_1} \left[\frac{1}{\sqrt{(x-\xi)^2 + (y-\eta)^2 + [z - z_0(\eta)]^2}} \right] d\xi\, d\sigma$$

Here ξ, η, σ are dummy variables replacing x, y, s in the wing surface, while n_1 is the normal direction at point ξ, η, $z_0(\eta)$. Subscripts U and L denote "upper" and "lower" sides of S relative to the n_1-direction (cf. Fig. 1). Combining Eqs. (10) and (11) yields the incompressible-flow integral equation

$$\frac{\partial \bar{m}}{\partial x} + i\omega \frac{\bar{m}}{U} = \frac{1}{4\pi\rho_\infty U^2} \iint_S [\overline{p_L} - \overline{p_U}]\, K\, d\xi\, d\sigma \qquad (12)$$

with the singular kernel function

$$K = \lim_{z \to z_0(y)} \left\{ e^{-i\frac{\omega}{U}(x-\xi)} \frac{\partial^2}{\partial n \partial n_1} \int_{-\infty}^{(x-\xi)} \frac{e^{i\frac{\omega\lambda}{U}}\, d\lambda}{\sqrt{\lambda^2 + (y-\eta)^2 + [z - z_0(\eta)]^2}} \right\} \qquad (13)$$

The double integral of Eq. (12) is to be evaluated in the sense of Mangler (Ref. 13), the principal singularity being associated with a factor $(y - \eta)^{-2}$. After some manipulation, which generalizes the work of Watkins, Runyan and Woolston (Ref. 14), a suitable working form of the kernel function is found to be

$$K = \sin[\theta(y)+\theta(\eta)]\frac{y_o z_{oo}}{r_1^4}\left\{\frac{x_o[3r_1^2+2x_o^2]}{r_o^3} - i\frac{\omega x_o^2}{U r_o}\right. \qquad (14)$$

$$-i\frac{\omega}{U}e^{-i\frac{\omega x_o}{U}}\int_0^{x_o}\frac{\lambda e^{i\frac{\omega\lambda}{U}}d\lambda}{\sqrt{\lambda^2+r_1^2}} - \frac{\omega^2}{U^2}e^{-i\frac{\omega x_o}{U}}\int_0^{x_o}\frac{\lambda^2 e^{i\frac{\omega\lambda}{U}}d\lambda}{\sqrt{\lambda^2+r_1^2}}$$

$$\left.+k_1^2 e^{-i\frac{\omega x_o}{U}}\left[K_2(k_1)-\frac{\pi i}{2}\left(I_2(k_1)-L_2(k_1)\right)+\frac{ik_1}{3}-\frac{i}{k_1}\right]\right\}$$

$$-\cos\theta(y)\cos(\eta)\frac{1}{r_1^2}\left\{\frac{y_o^2}{r_1^2}\left[-\frac{x_o}{r_o}+i\frac{\omega}{U}e^{-i\frac{\omega x_o}{U}}\int_0^{x_o}\frac{\lambda e^{i\frac{\omega\lambda}{U}}d\lambda}{\sqrt{\lambda^2+r_1^2}}\right]\right.$$

$$+\frac{z_{oo}^2}{r_1^2}\left[\frac{x_o[2r_1^2+x_o^2]}{r_o^3}-i\frac{\omega x_o^2}{U r_o}-\frac{\omega^2}{U^2}e^{-i\frac{\omega x_o}{U}}\int_0^{x_o}\frac{\lambda^2 e^{i\frac{\omega\lambda}{U}}d\lambda}{\sqrt{\lambda^2+r_1^2}}\right]$$

$$-k_1 e^{-i\frac{\omega x_o}{U}}\left[K_1(k_1)+\frac{\pi i}{2}\left(I_1(k_1)-L_1(k_1)\right)-i\right]$$

$$\left.+k_1^2\frac{z_{oo}^2}{r_1^2}e^{-i\frac{\omega x_o}{U}}\left[K_2(k_1)-\frac{\pi i}{2}\left(I_2(k_1)-L_2(k_1)\right)+\frac{ik_1}{3}-\frac{i}{k_1}\right]\right\}$$

$$-\sin\theta(y)\sin\theta(\eta)\frac{1}{r_1^2}\left\{\frac{z_{oo}^2}{r_1^2}\left[-\frac{x_o}{r_o}+i\frac{\omega}{U}e^{-i\frac{\omega x_o}{U}}\int_0^{x_o}\frac{\lambda e^{i\frac{\omega\lambda}{U}}d\lambda}{\sqrt{\lambda^2+r_1^2}}\right]\right.$$

$$+\frac{y_o^2}{r_1^2}\left[\frac{x_o[2r_1^2+x_o^2]}{r_o^3}-i\frac{\omega x_o^2}{U r_o}-\frac{\omega^2}{U^2}e^{-i\frac{\omega x_o}{U}}\int_0^{x_o}\frac{\lambda^2 e^{i\frac{\omega\lambda}{U}}d\lambda}{\sqrt{\lambda^2+r_1^2}}\right]$$

$$-k_1 e^{-i\frac{\omega x_o}{U}}\left[K_1(k_1)+\frac{\pi i}{2}\left(I_1(k_1)-L_1(k_1)\right)-i\right]$$

$$\left.+k_1^2\frac{y_o^2}{r_1^2}e^{-i\frac{\omega x_o}{U}}\left[K_2(k_1)-\frac{\pi i}{2}\left(I_2(k_1)-L_2(k_1)\right)+\frac{ik_1}{3}-\frac{i}{k_1}\right]\right\}$$

Here I_1, K_1 and L_1 are modified Bessel and Lommel functions in standard notation. The auxiliary symbols are as follows:

$$\left.\begin{aligned} x_o = x - \xi \quad , \quad y_o = y - \eta \quad , \quad z_{oo} = z_o(y) - z_o(\eta), \\ r_1 = \sqrt{y_o^2 + z_{oo}^2} \quad , \quad r_o = \sqrt{x_o^2 + y_o^2 + z_{oo}^2} \, , \\ b_1 = \frac{\omega r_1}{U} \end{aligned}\right\} \quad (15)$$

A generalization of the kernel function to include the influence of Mach number in subsonic compressible flow has been derived, but space considerations prevent reproducing it here. Several reformulations of Eq. (12) for special physical situations are discussed below:

a.) Pair or collection of non-intersecting lifting surfaces. In this case a boundary condition like Eq. (12) would be written for each surface and would contain integral terms on the right equal to the total number of surfaces, only the term representing the influence of a particular surface on itself involving a singular integration. One is thus required to solve a system of coupled integral equations for $[p_L - p_u]$ over all the interfering elements. K will have essentially the same form as Eq. (14) in all terms. The surfaces do not have to be plane or parallel.

b.) Intersecting lifting surfaces. This problem differs from the one described under a.) only because p_L and p_u on a surface may be discontinuous through the station where it is intersected by another. The solution procedure described below must be modified to permit these jumps but to assure continuity of pressure as the corner is turned from one surface onto another.

c.) Effect of a ground plane. By the well-known image principle, a ground plane (cf. Fig. 1) is accounted for by adding to the field an image which is loaded in a sense symmetrical to the original wing. The effect can be introduced as an additive correction to K in the single integral of Eq. (12).

d.) Effect of a free water surface on an oscillating hydrofoil running at high Froude number $F = U/\sqrt{g\ell}$. The boundary condition of constant pressure at the free surface z = d (Fig. 1) is known to reduce to $\varphi = 0$ when $F \gg 1$. This condition is met by loading the image in a sense antisymmetrical to the original wing, that is, by making $[\overline{p_L - p_u}]$ the same at corresponding points. The "upper" surface is the positive z-side in each case. Again, an additive correction to K appears in Eq. (12).

The steady-flow simplification of the kernel function is substantial:

$$y_o^2 K(\omega=0) = \sin[\theta(y)+\theta(\eta)]\frac{y_o^3 z_{oo}}{r_1^4}\left[2 + \frac{x_o[3r_1^2+2x_o^2]}{r_o^3}\right]$$

$$-\cos\theta(y)\cos\theta(\eta)\frac{y_o^2 z_{oo}^2}{r_1^4}\left[1 + \frac{x_o[2r_1^2+x_o^2]}{r_o^3} - \frac{y_o^2}{z_{oo}^2}\left(1+\frac{x_o}{r_o}\right)\right] \quad (16)$$

$$-\sin\theta(y)\sin\theta(\eta)\frac{y_o^4}{r_1^4}\left[1 + \frac{x_o[2r_1^2+x_o^2]}{r_o^3} - \frac{z_{oo}^2}{y_o^2}\left(1+\frac{x_o}{r_o}\right)\right]$$

The influence of Mach number in steady motion can be handled most simply by means of the Prandtl-Glauert compressibility correction.

Regardless of the physical circumstances, the numerical procedure which has been found most effective for solving integral equations like Eq. (12) is the same, a direct outgrowth of Watkins' development (Ref. 15) for planar wings. The key idea is to approximate $[\overline{p_L - p_u}]$ with a rapidly-convergent series of functions which give the right leading-edge singularity, fulfill the Kutta hypothesis along the trailing edge, and also drop to zero with the correct infinite slope along side edges. If the wingtips are located at $x = \pm B/2$, one introduces the following variables to transform S onto a rectangle between $\delta = -1, +1$ and $\theta = 0, \pi$:

$$\left.\begin{aligned} x &\doteq \tfrac{1}{2}[X_T(s) + X_L(s)] - \tfrac{1}{2}[X_T(s) - X_L(s)]\cos\theta \\ s &= \frac{B}{2}\delta \end{aligned}\right\} \quad (17)$$

Here x_T and x_L are streamwise coordinates of the leading and trailing edges, respectively. The pressure series reads

$$\overline{[p_L - p_U]} = 4\pi\rho_\infty U^2 \frac{B}{[x_T - x_L]} \sqrt{1-\delta^2} \cdot \left\{ \sum_{m=0} a_{0m} \delta^m \cot\frac{\theta}{2} + \sum_{n=1}\sum_{m=0} \frac{4}{2^{2n}} a_{nm} \delta^m \sin n\theta \right\} \quad (18)$$

(Several series are, of course, needed for a system of interfering surfaces.)

When Eq. (18) is inserted into Eq. (12), with dummy integration variables, the integrals can be evaluated numerically at a set of stations (x, s) on the half-span. For the assumed symmetrical planform shape, the loading is divided into symmetrical and antisymmetrical portions in a well-known way. Integrations must be performed with care because of the y_0^{-2} singularity; the work of Ref. 15 has proved very useful in this connection. The results may be cast in the matric form

$$[K]\{a_{nm}\} = \left\{ \left[\frac{\partial \bar{n}}{\partial x} + i\frac{\omega \bar{n}}{U} \right] \right\} \quad (19)$$

Here $\{\cdots\}$ are column matrices, whereas $[K]$ is a square or rectangular matrix, whose complex elements are integrals of the kernel weighted by individual terms in the series, Eq. (18). One solves for the column $\{a_{nm}\}$ of unknown coefficients by direct inversion or some least-squares technique. The load distribution comes from Eq. (18), and generalized forces like lift and pitching moment can often be expressed in terms of relatively few of the a_{nm}. Clearly, all of these steps would be unthinkable without high-speed digital computing machinery. The IBM 7090 at Massachusetts Institute of Technology is able, however, to solve one case of steady loading on a nonplanar wing or of unsteady loading on a planar wing in less than five minutes, nine to sixteen collocation points on the half-span being employed.

It should be mentioned, in passing, that more sophisticated schemes for solving Eq. (12) have been proposed and deserve further examination in the case of nonplanar surfaces. For instance, Hsu (Ref. 16 and antecedents) adopts the series (18) but simplifies the

integrations with a "natural" choice of collocation points. Stark (Ref. 17) has been able to avoid certain difficulties with rapidity of convergence by focussing on generalized-force computation, using reverse-flow theorems, and introducing least squares when applying the flow-tangency boundary condition.

Illustrative solutions of Eq. (12) for a variety of practical problems are presented by Figs. 2 through 7. In each instance the fluid is of constant density, since most applications to date have been carried out in connection with hydrofoil design. Many similar results for planar surfaces in both compressible and incompressible flow will be found in Refs. 18, 16, 17 etc.

Figure 2, adapted from a recent study of ground effect by Saunders (Ref. 19) demonstrates the excellent accuracy that can often be obtained at low incidence even on quite thick wings. The reader is directed to Ref. 19 for sources and interpretation of the data. Shown plotted vs. height above ground in chords, the ordinate is dimensionless lift per radian of angle of attack for three rectangular surfaces:

$$C_L \equiv \frac{L}{\frac{\rho_\infty}{2} U^2 S} = \frac{1}{S} \iint_S \frac{[p_L - p_U]}{\frac{\rho_\infty}{2} U^2} dx ds \qquad (20)$$

The dimensionless nose-up pitching moments, associated with these lifts, about a spanwise axis 25% of the way back from the leading edge are graphed in Fig. 3. The ground plane's influence is seen to cause an increase in lift while displacing its center of action aft. As an example of combined ground and non-planar effects, Fig. 4 plots lift-curve slope for a V-wing at different heights and dihedral angles.

Figures 5 - 7 concern oscillatory motion in the presence of a free surface, 5 and 6 being taken from a recent paper by the author and two colleagues (Ref. 20). In Fig. 5, the vibration consists of a vertical translation

$$\Delta z(x, y, t) = -\bar{h} e^{i\omega t} , \qquad (21)$$

while Fig. 6 refers to nose-up pitch-angle displacement $\propto e^{i\omega t}$ about the quarter-chord axis. The abscissa is reduced frequency, Eq. (6), with length l chosen to equal the semichord b. Being complex numbers, the dimensionless aerodynamic loads are shown in magnitude and phase-angle form, e.g.,

$$C_L = |C_L| e^{i\varphi_L} = C_{L_R} + i\, C_{L_I} \tag{22}$$

Froude number in Figs. 5 and 6 is assumed large enough to permit use of the antisymmetrical image wing. Geometrical characteristics are listed on the figures.

The calculations in Fig. 7, previously unpublished, refer to the two-dimensional hydrofoil running at finite Froude number. The integral of Eq. (12) is here replaced by a single integration along the chord, but the kernel function (Ref. 20) must account for the various trains of surface waves set up by the motion. The important parameter of this problem is

$$k F^2 = \frac{\omega U}{g} \tag{23}$$

One sees the singular behavior near $kF^2 = 0.25$ that was discussed by Crimi and Statler (Ref. 21). $F = 10$ is evidently large enough, however, to permit the infinite-Froude-number approximation for practical reduced frequencies.

No subsonic interacting systems containing bodies have been successfully worked through by the methods of this report. It is expected that recourse will have to be taken to fundamental representations, in terms of source and doublet solutions of the governing differential equation distributed over all surfaces bounding the flow. The circumstances where complete linearization is permissible, especially for pressure calculation, are by no means as clear as when only lifting surfaces are involved. Although this may seem to be a very complicated undertaking, yet it is dangerous to underestimate the potential of digital computers for well-stated, highly systematized problems. One need only call attention to the pioneering achievements by Smith and collaborators, of which Ref. 22 is an early example, on large-disturbance incompressible flows around bodies of arbitrary shape without circulation.

III. Slender Configurations at Supersonic Speed.

When $M>1$ the character of phenomena described by Eq. (3) changes as a consequence of the inability of signals to propagate upstream. Although it is still possible to construct a kernel function for Eq. (12), and important work has been done in this direction, the author believes that a more fruitful approach to interference problems lies via the inverted representation of the solution and the method of aerodynamic influence coefficients (AIC's, Refs. 23 and 24).

The AIC scheme is founded on an artificiality that brings about both a great deal of mathematical simplification and some difficulty in physical understanding. This is the use of source sheets, which produce symmetrical flow with respect to the wing plane, in place of doublet sheets having the expected lifting antisymmetry. A necessary accompaniment to sources is the addition of hypothetical "diaphragm" areas, whose purpose is to isolate opposite sides of lifting surfaces while ensuring that no load acts on regions which cannot sustain it. Thickness effects are, incidentally, omitted also from the present treatment of the supersonic case, but they are easily superimposed as mentioned at the beginning of Section II.

By way of introduction to AIC's, the procedure for finding the flow due to a vibrating plane configuration like that in Fig. 8 is briefly reviewed. The disturbance potential at any (x, y, z) in the half-space $z \geq 0$ is given by (Refs. 7, 23, etc.)

$$\bar{\Phi}(x,y,z) = R.P.\left\{-\frac{1}{\pi}\iint_S \frac{\bar{w}(\xi,\eta)\, e^{-i\frac{\omega M^2(x-\xi)}{U\beta^2}} \cos\left(\frac{\omega M}{U\beta^2}\sqrt{(x-\xi)^2-\beta^2[(y-\eta)^2+z^2]}\right)}{\sqrt{(x-\xi)^2-\beta^2[(y-\eta)^2+z^2]}}\, d\xi\, d\eta\right\} \quad (24)$$

Here $\beta \equiv \sqrt{M^2-1}$; $\bar{w}$ is proportional to source strength per unit area and here equals the vertical velocity induced by the source sheet just above the surface. The operator R. P. calls for taking the real part only with respect to the change in sign of the quantity under the radical. When this operation is performed, S reduces to that portion of the wing-diaphragm area intercepted by the upstream Mach cone from (x, y, z).

As in the figure, wing and diaphragm are overlaid to the closest possible approximation with elementary areas (b_1 by b_1/β rectangles) having diagonals parallel to the Mach lines. In terms of the dimensionless quantities

$$\left.\begin{aligned} x_1, \xi_1 &= \frac{x, \xi}{b_1} \\ y_1, \eta_1, z_1 &= \frac{y, \eta, z}{b_1/\beta} \\ \bar{k}_1 &= \frac{\omega b_1}{U}\frac{M^2}{\beta^2} \end{aligned}\right\} \qquad (25)$$

Eq. (24) reads

$$\bar{\Phi}(x_1, y_1, z_1) \qquad (26)$$

$$= R.P.\left\{-\frac{b_1}{\pi\beta}\iint_{S_1}\frac{\bar{w}(\xi_1,\eta_1)\, e^{-i\bar{k}_1(x_1-\xi_1)}\cos\left(\frac{\bar{k}_1}{M}\sqrt{(x_1-\xi_1)^2-(y_1-\eta_1)^2-z_1^2}\right)}{\sqrt{(x_1-\xi_1)^2-(y_1-\eta_1)^2-z_1^2}}\, d\xi_1 d\eta_1\right\}$$

Now let it be assumed (as will be correct in the limit $b_1 \to 0$) that $\bar{w}$ is constant over each element and equal to the value $\bar{w}_{\nu,\mu}$ at the center. By placing the origin at the foremost of these centers, ν and μ are caused to be integers counting centers rearward and to the right from this origin. The potential may be written

$$\bar{\Phi}(x_1, y_1, z_1) = \frac{b_1}{\beta}\sum_{\nu,\mu} \bar{\Phi}_{\nu,\mu}(x_1, y_1, z_1)\, \bar{w}_{\nu,\mu} \quad , \qquad (27)$$

where the sum is extended over all elements ahead of or along the hyperbolic intersection between z = 0 and the forward Mach cone. Making the substitutions

$$\left.\begin{aligned} \bar{\nu} &= x_1 - \nu \\ \bar{\mu} &= y_1 - \mu \\ z_1 &= \ell \end{aligned}\right\} \qquad (28)$$

it is an easy matter to show that the AIC $\bar{\Phi}_{\nu,\mu}(x_1, y_1 z_1)$ actually depends only on the relative position between the "sending" area and "receiving" point. Indeed, it can be expressed as

$$\Phi_{\bar{\nu},\bar{\mu},\ell} = R.P.\left\{-\frac{1}{\pi}\int_{(\bar{\nu}-\frac{1}{2})}^{(\bar{\nu}+\frac{1}{2})}\int_{(\bar{\mu}-\frac{1}{2})}^{(\bar{\mu}+\frac{1}{2})} \frac{e^{-i\bar{k}_1\bar{\xi}_1}\cos\left(\frac{\bar{k}_1}{M}\sqrt{\bar{\xi}_1^2-\bar{\eta}_1^2-\ell^2}\right)}{\sqrt{\bar{\xi}_1^2-\bar{\eta}_1^2-\ell^2}}\,d\bar{\eta}_1\,d\bar{\xi}_1\right\} \quad (29)$$

where $\bar{\xi}_1 = (x_1 - \xi_1)$ and $\bar{\eta}_1 = (y_1 - \eta_1)$.

In a similar fashion, the velocity components $\bar{v} = \bar{\phi}_y$ and $\bar{w} = \bar{\phi}_z$ at a field point can be obtained from

$$\bar{v}(x_1, y_1, z_1) = \sum_{\nu,\mu} V_{\bar{\nu},\bar{\mu},\ell}\,\bar{w}_{\nu,\mu} \quad (30)$$

$$\bar{w}(x_1, y_1, z_1) = \sum_{\nu,\mu} W_{\bar{\nu},\bar{\mu},\ell}\,\bar{w}_{\nu,\mu} \quad (31)$$

V and W being essentially y and z derivatives of the quantity in Eq. (29). Formulas have been worked out for numerically computing various AIC's along the lines of Ref. 24. Although space does not permit discussing all the complications brought on by Mach-cone intersections, the basic forms for "uncut" area elements are reproduced below ($\bar{\nu} > 0$, $\bar{\mu} > 0$):

$$\Phi_{\bar{\nu},\bar{\mu},\ell} = R.P.\left\{\frac{1}{\pi}\int_{\bar{\nu}-\frac{1}{2}}^{\bar{\nu}+\frac{1}{2}} e^{-i\bar{k}_1\bar{\xi}_1}\left[J_0\left(\frac{\bar{k}_1}{M}\sqrt{\bar{\xi}_1^2-\ell^2}\right)\sin^{-1}\left(\frac{\bar{\mu}-\frac{1}{2}}{\sqrt{\bar{\xi}_1^2-\ell^2}}\right)\right.\right. \quad (32)$$

$$\left. - J_0\left(\frac{\bar{k}_1}{M}\sqrt{\bar{\xi}_1^2-\ell^2}\right)\sin^{-1}\left(\frac{\bar{\mu}+\frac{1}{2}}{\sqrt{\bar{\xi}_1^2-\ell^2}}\right) + 2\sum_{r=1}^{} \frac{(-1)^r}{2r} J_{2r}\left(\frac{\bar{k}_1}{M}\sqrt{\bar{\xi}_1^2-\ell^2}\right)\cdot\right.$$

$$\left.\cdot\left\langle \sin\left(2r\sin^{-1}\frac{\bar{\mu}-\frac{1}{2}}{\sqrt{\bar{\xi}_1^2-\ell^2}}\right) - \sin\left(2r\sin^{-1}\frac{\bar{\mu}+\frac{1}{2}}{\sqrt{\bar{\xi}_1^2-\ell^2}}\right)\right\rangle\right]d\bar{\xi}_1\Bigg\}$$

$$V_{\bar{\nu},\bar{\mu},\ell} = R.P.\left\{\frac{1}{\pi}\int_{\bar{\nu}-\frac{1}{2}}^{\bar{\nu}+\frac{1}{2}} e^{-i\bar{k}_1\bar{\xi}_1}\left[\frac{\cos\left(\frac{\bar{k}_1}{M}\sqrt{\bar{\xi}_1^2-(\bar{\mu}-\frac{1}{2})^2-\ell^2}\right)}{\sqrt{\bar{\xi}_1^2-(\bar{\mu}-\frac{1}{2})^2-\ell^2}}\right.\right. \quad (33)$$

$$\left.\left. - \frac{\cos\left(\frac{\bar{k}_1}{M}\sqrt{\bar{\xi}_1^2-(\bar{\mu}+\frac{1}{2})^2-\ell^2}\right)}{\sqrt{\bar{\xi}_1^2-(\bar{\mu}+\frac{1}{2})^2-\ell^2}}\right]d\bar{\xi}_1\right\}$$

$$W_{\bar{\nu},\bar{\mu},\ell} = W^{(2)}_{\bar{\nu},\bar{\mu},\ell} - W^{(1)}_{\bar{\nu},\bar{\mu},\ell} \quad ,$$

where (34A)

$$W^{(2)}_{\bar{\nu},\bar{\mu},\ell} = R.P.\left\{ \frac{\ell}{\pi} \int_{\bar{\nu}-\frac{1}{2}}^{\bar{\nu}+\frac{1}{2}} e^{-i\bar{k}_1\bar{\xi}_1} \left[\frac{(\bar{\mu}-\frac{1}{2})\cos\left(\frac{\bar{k}_1}{M}\sqrt{\bar{\xi}_1^2-(\bar{\mu}-\frac{1}{2})^2-\ell^2}\right)}{(\bar{\xi}_1^2-\ell^2)\sqrt{\bar{\xi}_1^2-(\bar{\mu}-\frac{1}{2})^2-\ell^2}} \right.\right.$$

$$+ \frac{2}{(\bar{\xi}_1^2-\ell^2)} \sum_{r=1} (-1)^r J_{2r}\left(\frac{\bar{k}_1}{M}\sqrt{\bar{\xi}_1^2-\ell^2}\right) \sin\left(2r \sin^{-1}\frac{\bar{\mu}-\frac{1}{2}}{\sqrt{\bar{\xi}_1^2-\ell^2}}\right)$$

$$+ \frac{\bar{k}_1}{M} \frac{J_1\left(\frac{\bar{k}_1}{M}\sqrt{\bar{\xi}_1^2-\ell^2}\right)}{\sqrt{\bar{\xi}_1^2-\ell^2}} \sin^{-1}\left(\frac{\bar{\mu}-\frac{1}{2}}{\sqrt{\bar{\xi}_1^2-\ell^2}}\right) - \frac{2\bar{k}_1}{M\sqrt{\bar{\xi}_1^2-\ell^2}} \sum_{r=1} \frac{(-1)^r}{2r} J_{2r-1}\left(\frac{\bar{k}_1}{M}\sqrt{\bar{\xi}_1^2-\ell^2}\right) \cdot$$

$$\left.\left. \cdot \sin\left(2r \sin^{-1}\frac{\bar{\mu}-\frac{1}{2}}{\sqrt{\bar{\xi}_1^2-\ell^2}}\right) \right] d\bar{\xi}_1 \right\}$$

(34B)

and $W^{(1)}_{\bar{\nu},\bar{\mu},1}$ has the same form except that $(\bar{\mu} - 1/2)$ is replaced by $(\bar{\mu} + 1/2)$. Symmetry considerations can be used to establish that $\Phi_{\bar{\nu},-\bar{\mu},\ell} = \Phi_{\bar{\nu},\bar{\mu},\ell}$,

$V_{\bar{\nu},-\bar{\mu},\ell} = -V_{\bar{\nu},\bar{\mu},\ell}$, $V_{\bar{\nu},0,\ell} = 0$, $W_{\bar{\nu},-\bar{\mu},\ell} = W_{\bar{\nu},\bar{\mu},\ell}$, etc.

In practice, the single integrals in Eqs. (32) - (34) must be evaluated by quadrature. This gives rise to no serious difficulties, and conveniently isolated computer subroutines have been successfully operated for each of the AIC's (for example, by North American Aviation, Inc.*).

---

* Work of Andrew and collaborators, as yet unpublished.

The use of AIC's for loading calculation on a plane wing is described, with rules based on extensive experience, in Refs. 24. In most cases, all design information can be determined from the distribution of $\bar{\varphi}$ over the planform, so that only Eq. (27) and the velocity potential AIC (Eq. (33) with $l = 0$) are used. $\bar{\varphi}(x_1, y_1, 0)$ is calculated sequentially at centers of area elements, starting from (0,0) in Fig. 8. For the summation in Eq. (27), $\bar{w}_{y,\mu}$ is known, in terms of the motion, at points on the planform and can be determined from the condition $\bar{\varphi} = 0$ at points on the diaphragm region, shaded in the figure. If the steps are performed in the proper order, it is never necessary to solve any systems of simultaneous equations or invert matrices.

Figure 9, adapted from Ref. 24, gives an example of the AIC estimation of spanwise lift distribution at a rectangular wingtip compared with series-expansion results obtained by Watkins (Ref. 25). This figure also demonstrates the improved accuracy which can be achieved by introducing additional terms to account for the singularity of upwash that exists just off the side edge where the diaphragm meets the wing (Ref. 24). The inclusion of such singularities at leading and side edges has been examined in detail. As a general conclusion, it appears that comparable accuracy can be obtained in the φ-distribution at less computational cost by dispensing with these special terms and reducing the area-element size relative to the wing dimensions. Although mathematically less rigorous, this approach is tentatively being taken with interfering surfaces as well.

Procedures for applying AIC's to nonplanar wings and interfering wing-body systems have been outlined by the author in an unpublished report (Ref. 26). Two examples are presented here to illustrate the principles. Consider first a single nonplanar surface of the sort shown in Fig. 10, oscillating in a known mode of vibration. From Eq. (9), v_n will be spedified over the planform area S. To assure no communication between upper and lower surfaces, plane diaphragm areas are associated with both the main wing and bent-down wingtip, each extending out to meet the Mach cone from the vertex. A vertical plane of symmetry is assumed at the vehicle centerline, so that it is necessary to work over only half the planform, making automatic provisions to account for contributions from the opposite half. Clearly, the two tips do not interact.

Area elements like those in Fig. 8 are distributed over the upper and lower sides of all lifting and diaphragm regions, and oscillatory sources of constant amplitude are placed on each element. Let $\bar{S}^{(\ell)}$ and $\bar{S}^{(k)}$ denote source-strength amplitude per unit area of the upper and lower sides, respectively, of the main wing and its diaphragm. $\bar{S}^{(t)}$ and $\bar{S}^{(k_t)}$ are corresponding strengths for the tip and tip diaphragm. The physical conditions to be met are 1.) that $\bar{\nu}_m$ have the correct values on lifting area elements, and 2.) that both $\bar{\nu}_m$ and pressure ($\bar{\varphi}$ in this case) be continuous through each diaphragm element. For example, the normal velocity at points on upper wing area i induced by the sources on j can be written

$$\bar{\nu}_m^{(ij)}(\bar{x}_i, \bar{y}_i, \ell_i) = \sum_{\bar{\nu}_j, \mu_j} \left[W_{\bar{\nu}, \bar{\mu}, \ell} \cos\theta - V_{\bar{\nu}, \bar{\mu}, \ell} \sin\theta \right] \bar{S}^{(j)}(\nu_j, \mu_j, \ell_j) \tag{35}$$

Care must be taken with the definitions of $\bar{\nu}, \bar{\mu}, \ell$ here. $\bar{\nu}$ is the dimensionless chordwise distance aft from the center of the "sending" j-element to the "receiving" i-element, whereas $\bar{\mu}$ and ℓ are dimensionless relative distances measured tangential and normal to the plane of wingtip j. Centers can usually be chosen so that $\bar{\nu}$ is always an integer, but $\bar{\mu}, \ell$ will be irrational numbers (ℓ is here negative).

Equation (35) can be recast, in obvious matric notation, as

$$\left\{ \bar{\nu}_m^{(ij)} \right\}_W = \left(\cos\theta \left[W_{\bar{\nu}, \bar{\mu}, \ell}^{(ij)} \right] - \sin\theta \left[V_{\bar{\nu}, \bar{\mu}, \ell}^{(ij)} \right] \right) \left\{ \bar{S}^{(j)} \right\}_{WD} \tag{36}$$

Subscript "W" on the left-hand column matrix indicates that only area-element centers on the lifting portion of the wing are included, while "WD" on the right means that all wingtip and wingtip-diaphragm elements are represented. The rectangular matrices on the right will contain many zeroes due to the law of forbidden signals, and there is an advantage to properly ordering the computations. The normal velocity at points on area j from the presence of sources on the upper side of the wing and its diaphragm is

$$\left\{\bar{v}_n^{(j,i)}\right\}_W = \left(\cos\theta\left[W^{(j,i)}_{\bar{\nu},\bar{\mu},\ell}\right] + \sin\theta\left[V^{(j,i)}_{\bar{\nu},\bar{\mu},\ell}\right]\right)\left\{\bar{S}^{(i)}\right\}_{WD} \quad (37)$$

where $\bar{\nu}$, $\bar{\mu}$, ℓ are now referred to the wing's plane.

Given the normal-velocity amplitudes $\bar{v}_n^{(j)}$ and $\bar{v}_n^{(i)}$ produced by the known motion of wing and tip, the geometrical boundary conditions on these upper lifting areas read

$$\left\{\bar{S}^{(i)}\right\}_W = \left\{\bar{v}_n^{(i)}\right\}_W - \left\{\bar{v}_n^{(i,j)}\right\}_W = \left\{\bar{v}_n^{(i)}\right\}_W \quad (38)$$
$$-\left(\cos\theta\left[W^{(i,j)}_{\bar{\nu},\bar{\mu},\ell}\right] - \sin\theta\left[V^{(i,j)}_{\bar{\nu},\bar{\mu},\ell}\right]\right)\left\{\bar{S}^{(j)}\right\}_{WD}$$

$$\left\{\bar{S}^{(j)}\right\}_W = \left\{\bar{v}_n^{(j)}\right\}_W - \left\{\bar{v}_n^{(j,i)}\right\}_W = \left\{\bar{v}_n^{(j)}\right\}_W \quad (39)$$
$$-\left(\cos\theta\left[W^{(j,i)}_{\bar{\nu},\bar{\mu},\ell}\right] + \sin\theta\left[V^{(j,i)}_{\bar{\nu},\bar{\mu},\ell}\right]\right)\left\{\bar{S}^{(i)}\right\}_{WD}$$

There are two essentially identical relations for the lower surface, superscripts (i) and (j) being replaced with (ℓ) and (k), respectively.

The kinematic conditions of continuity of normal velocity across the two diaphragms read

$$\left\{\bar{S}^{(i)}\right\}_D + \left\{\bar{v}_n^{(i,j)}\right\}_D = -\left(\left\{\bar{S}^{(\ell)}\right\}_D + \left\{\bar{v}_n^{(\ell,k)}\right\}_D\right) \quad (40)$$

$$\left\{\bar{S}^{(j)}\right\}_D + \left\{\bar{v}_n^{(j,i)}\right\}_D = -\left(\left\{\bar{S}^{(k)}\right\}_D + \left\{\bar{v}_n^{(k,\ell)}\right\}_D\right) \quad (41)$$

Here substitutions like Eqs. (36) and (37), modified to refer to diaphragm rather than wing area elements, are used to eliminate the interference matrices and write Eqs. (40) - (41) entirely in terms of source strengths.

An additional set of equations covering the diaphragm centers is needed to construct a determinate system. This is provided by the requirement of pressure continuity, which is equivalent to $\bar{\Phi}$-continuity in the present case. Thus,

$$\frac{\beta}{b_1}\left\{\bar{\Phi}^{(i)}\right\}_D \equiv \left[\Phi^{(ii)}_{\bar{\nu},\bar{\mu},0}\right]\left\{\bar{S}^{(i)}\right\}_{WD} + \left[\Phi^{(ij)}_{\bar{\nu},\bar{\mu},\ell}\right]\left\{\bar{S}^{(j)}\right\}_{WD} \tag{42}$$

$$= \frac{\beta}{b_1}\left\{\bar{\Phi}^{(\ell)}\right\}_D \equiv \left[\Phi^{(\ell\ell)}_{\bar{\nu},\bar{\mu},0}\right]\left\{\bar{S}^{(\ell)}\right\}_{WD} + \left[\Phi^{(\ell k)}_{\bar{\nu},\bar{\mu},\ell}\right]\left\{\bar{S}^{(k)}\right\}_{WD}$$

$$\frac{\beta}{b_1}\left\{\bar{\Phi}^{(j)}\right\}_D \equiv \left[\Phi^{(jj)}_{\bar{\nu},\bar{\mu},0}\right]\left\{\bar{S}^{(j)}\right\}_{WD} + \left[\Phi^{(ji)}_{\bar{\nu},\bar{\mu},\ell}\right]\left\{\bar{S}^{(i)}\right\}_{WD}$$

$$= \frac{\beta}{b_1}\left\{\bar{\Phi}^{(k)}\right\}_D \equiv \left[\Phi^{(kk)}_{\bar{\nu},\bar{\mu},0}\right]\left\{\bar{S}^{(k)}\right\}_{WD} + \left[\Phi^{(k\ell)}_{\bar{\nu},\bar{\mu},\ell}\right]\left\{\bar{S}^{(\ell)}\right\}_{WD} \tag{43}$$

The total of the linear equations can now be proved to equal the number of unknown area-element source strengths. Experience at North American Aviation, Inc., has shown that the foregoing computation can be successfully mechanized and that skillful ordering avoids the need for matrix inversions. Once the unknowns have been determined, equations like the following will yield $\bar{\Phi}$ on each side of each lifting surface:

$$\left\{\bar{\Phi}^{(i)}\right\}_W = \frac{b_1}{\beta}\left(\left[\Phi^{(ii)}_{\bar{\nu},\bar{\mu},0}\right]\left\{\bar{S}^{(i)}\right\}_{WD} + \left[\Phi^{(ij)}_{\bar{\nu},\bar{\mu},\ell}\right]\left\{\bar{S}^{(j)}\right\}_{WD}\right) \tag{44}$$

Pressures and generalized forces can be found from $[\bar{\Phi}_L - \bar{\Phi}_U]$ as for planar wings. An example of the influence of tip deflection on lift and aerodynamic-center location is shown in Fig. 11. The AIC predictions are seen to follow measured trends quite satisfactorily.

As a second example, the hypersonic glider pictured in Fig. 12 is selected. No detailed calculations have yet been carried through on such an elaborate configuration, which includes a body, but the procedure is not essentially more complicated than for the nonplanar wing. The figure shows, shaded, a suitable system of diaphragms to prevent communication between the opposite sides of all thin surfaces.

As before, each side of each diaphragm and lifting region would be overlaid with rectangular area elements. Similar elements, also covered with constant-strength oscillating sources, are affixed in a suitable pattern over the body or fuselage. (The body base, being in a separated flow region, must be treated empirically, but conditions at this base cannot affect the loading forward.)

The illustrated fuselage is made up from essentially planar areas. Each of these can be treated exactly like one side of a lifting surface, with a flow-tangency boundary equation being available to determine the source strength on each area element. Were the body composed of curved surfaces, however, the normal direction for each separate planar element would have to be found and carried through the computation. Airload determination would then be somewhat more complicated, because each element over the entire body will receive normal velocity contributions from all others. There is no theoretical reason, however, why such interference problems involving bodies cannot be mechanized in a way that closely parallels systems with lifting surfaces only. Finally, it should be remarked that means for dealing with wakes arising from subsonic trailing edges are well-understood and can be deduced from the discussion and examples of Zartarian and Hsu (Ref. 24).

IV. Oscillatory Motion in Sonic Flight

As set forth in Ref. 11 and elsewhere, finite lifting surfaces flying near M = 1 are not susceptible of steady linearized treatment, but when $k \gg |1-M|$ the linear differential equation

$$\bar{\Phi}_{yy} + \bar{\Phi}_{zz} - \frac{2i\omega M}{U}\bar{\Phi}_x + \frac{\omega^2 M^2}{U^2}\bar{\Phi} = 0 \qquad (45)$$

governs the oscillatory field. This observation suggested to the author the possibility that the concept of AIC's might be adapted to sonic flight. Should such an approximation prove practical, the results can readily be extended to cover the "transonic range" between, say, M = 0.95 and 1.10 by means of Landahl's similarity law

$$\bar{\Phi}(x, y, z; M, k) = \frac{1}{M}\bar{\Phi}(x, My, Mz; M=1, k) \qquad (46)$$

The scheme which has undergone preliminary examination is suggested in Fig. 13. Here square area elements, each with constant oscillating source strength, are distributed over the planform and diaphragm regions of a planar wing. The Mach lines at sonic speed are parallel to the y-axis, so the diaphragms theoretically extend to infinity. One must therefore assume the normal velocity $\bar{w}_{y,n}$ arbitrarily equal to zero for diaphragm elements beyond a certain distance away from each wingtip. In Fig. 14 some analytical results for $\bar{w}$ off a rectangular tip in plunging vibration are plotted to suggest that this assumption is probably quite acceptable and that the necessary distance is a matter of a small number of chordlengths. Figure 14 was computed, incidentally, using the closed-form solution for a "quarter-infinite" wing on $x > 0$, $y > 0$ (Chap. VI of Ref. 11), from which one can deduce

$$\bar{\Phi}_z(x, y \leq 0; 0) \qquad (47)$$

$$= \frac{i\omega\bar{h}}{\sqrt{\pi}\,\Gamma(\frac{1}{4})}\,\frac{\ell\, e^{i\left(\frac{\pi}{8} - \frac{\omega x}{2U}\right)}}{x\sqrt{|y|}}\sqrt[4]{\frac{2Ux}{\omega}}\int_{\frac{\omega y^2}{2Ux}}^{\infty}\frac{\left[q - \frac{\omega y^2}{2Ux}\right]^{1/4} e^{-iq}\,dq}{q^{3/4}}$$

In Eq. (47) $\bar{h}$ is again the amplitude of vertical displacement, and q is a dummy variable of spanwise integration.

The formula for potential field which forms the sonic counterpart of Eq. (26) is readily found from Ref. 11 to read

$$\bar{\Phi}(x_1, y_1, z_1) = -\frac{b_1}{\pi}\int_0^{x_1}\int_{-\infty}^{\infty} \bar{w}(\xi_1, \eta_1)\, \frac{\exp\left[-i\frac{k_1}{2}(x_1-\xi_1) - i\frac{k_1}{2}\frac{(y_1-\eta_1)^2+z_1^2}{(x_1-\xi_1)}\right]}{[x_1-\xi_1]}\, d\eta_1 d\xi_1 \quad (48)$$

The dimensionless coordinates here are referred to side b_1 of the square elements and $k_1 = \omega b_1/U$. Under the restriction $\bar{y} \geq 0$, Eqs. (30) and (31) may be adopted without change, and Eq. (27) is replaced by

$$\bar{\Phi}(x_1, y_1, z_1) = -b_1 \sum_{\nu,\mu} \bar{w}_{\nu,\mu}\, \Phi^{(1)}_{\nu,\mu,\ell} \quad (49)$$

Except for easily-handled singular cases which occur when $\bar{y} = 0$, the AIC's are as follows (superscript (1) is used to denote sonic flow):

$$\Phi^{(1)}_{\nu,\mu,\ell} = \frac{1}{2\sqrt{\pi k_1}}\int_{\nu-\frac{1}{2}}^{\nu+\frac{1}{2}} e^{-i\frac{k_1}{2}\left(\bar{\xi}_1+\frac{\ell^2}{\bar{\xi}_1}\right)}\left[C\left(\frac{k_1}{2\bar{\xi}_1}(\mu+\tfrac{1}{2})^2\right) - C\left(\frac{k_1}{2\bar{\xi}_1}(\mu-\tfrac{1}{2})^2\right) + iS\left(\frac{k_1}{2\bar{\xi}_1}(\mu-\tfrac{1}{2})^2\right) - iS\left(\frac{k_1}{2\bar{\xi}_1}(\mu+\tfrac{1}{2})^2\right)\right]\frac{d\bar{\xi}_1}{\sqrt{\bar{\xi}_1}} \quad (50)$$

$$V^{(1)}_{\nu,\mu,\ell} = \frac{1}{2\pi}\int_{\nu-\frac{1}{2}}^{\nu+\frac{1}{2}}\left\{\exp\left[-i\frac{k_1}{2}\left(\bar{\xi}_1+\frac{\ell^2+(\mu-\frac{1}{2})^2}{\bar{\xi}_1}\right)\right] - \exp\left[-i\frac{k_1}{2}\left(\bar{\xi}_1+\frac{\ell^2+(\mu+\frac{1}{2})^2}{\bar{\xi}_1}\right)\right]\right\}\frac{d\bar{\xi}_1}{\bar{\xi}_1} \quad (51)$$

$$W^{(1)}_{\nu,\mu,\ell} = \frac{i\ell}{2}\sqrt{\frac{k_1}{\pi}}\int_{\nu-\frac{1}{2}}^{\nu+\frac{1}{2}} e^{-i\frac{k_1}{2}\left(\bar{\xi}_1+\frac{\ell^2}{\bar{\xi}_1}\right)}\left[C\left(\frac{k_1}{2\bar{\xi}_1}(\mu+\tfrac{1}{2})^2\right) - C\left(\frac{k_1}{2\bar{\xi}_1}(\mu-\tfrac{1}{2})^2\right) + iS\left(\frac{k_1}{2\bar{\xi}_1}(\mu-\tfrac{1}{2})^2\right) - iS\left(\frac{k_1}{2\bar{\xi}_1}(\mu+\tfrac{1}{2})^2\right)\right]\frac{d\bar{\xi}_1}{\bar{\xi}_1^{3/2}} \quad (52)$$

The notation adopted in Eqs. (50) - (52) for the Fresnel integrals is most conveniently expressed as

$$\left.\begin{aligned} C\left(\frac{\pi X^2}{2}\right) &\equiv \int_0^X \cos\left(\frac{\pi}{2}\xi^2\right) d\xi \\ S\left(\frac{\pi X^2}{2}\right) &\equiv \int_0^X \sin\left(\frac{\pi}{2}\xi^2\right) d\xi \end{aligned}\right\} \qquad (53)$$

All single integrations will have to be carried out numerically, but computer subroutines are already available for the Fresnel integrals. $\Phi^{(1)}_{\bar{y},\bar{z},0}$ has already been evaluated with enough accuracy and speed to assure the feasibility of airload determinations for nonplanar configurations.

The only numerical application of sonic AIC's known at present to author consists of an effort by the Boeing Company* to compare the surface distribution of $\bar{\varphi}$ against the well-known exact solution for two-dimensional flow. A few results are presented in Fig. 15. The wing, performing plunging oscillations at $k_1 = 0.05$, is intended to have infinite span, but the contributions to $\bar{\varphi}$ from points more than 80 area elements distant from the chordwise cross-section under consideration were neglected. As the computation proceeds downstream, the effective reduced frequency k (based on wing chordlength ahead) increases while the "aspect ratio" of the rectangular area by which the actual two-dimensional wing is approximated decreases. Since there is no reason to anticipate computational difficulty at higher k in this range, the ultimate deviation between the exact and AIC results can be attributed to the latter effect. Additional studies show poorer agreement at very low values of k, where linearized theory itself is questionable, but no practical difficulty is anticipated either with the total number of area elements or with excessive spanwise dimensions of the region which must be covered with them.

Because of the tendency of strong shocks to form at intermediate chordwise stations in transonic flow, very severe limitations will have to be placed on thickness- amplitude ratios and k will have to be relatively large before the foregoing theory will be valid for applications. It may, for example, prove useful only for flutter analyses rather than loads estimation. This is especially true on surfaces with

---

* Work of Weatherill, as yet unpublished.

nearly unswept leading edges. It is therefore important for this speed regime that Landahl (Ref. 28) and others are beginning to point the way toward suitable theoretical refinements.

V. Remarks on Special Topics; Conclusions

a.) Arbitrary Time-Dependent Motion

Aerodynamic loads due to sinusoidal vibration of interfering systems, predicted according to the methods of this paper, have immediate utility in flutter analyses and when determining the transfer functions of a flight vehicle for such harmonic inputs as sinusoidal gust velocity or displacement of the control surfaces. Instances frequently arise, however, when it would be advantageous to get loads directly for more general time-dependent motions. At low frequencies, of course, one can make the quasi-steady approximation and use the foregoing theories with $k = 0$. In situations such as rapid maneuvers, impulsive inputs, and transient structural vibrations this is often not permissible.

The author has given considerable thought to the engineering of unsteady aerodynamics for nonsinusoidal phenomena. He has concluded that, when elaborate theory is to be used in connection with high-speed digital computation, the most efficient approach lies through Fourier series decomposition of the inputs and responses. First successfully mechanized by Bisplinghoff et al. in 1949 (Ref. 29) for aircraft problems, this scheme has appeared in a number of versions including numerical evaluation of the Fourier integral by division into finite frequency intervals and truncation. Whatever the form, success seems to depend on retaining a rather large number of terms in the summations, which is something that can readily be systematized on a machine like the IBM 7090. As an illustration, North American Aviation* has been able to determine flexible-airframe response to standardized design gust shapes, representing the gust as a periodic input with quiescent intervals. Three-dimensional unsteady aerodynamics were employed in a seven-degree-of-freedom modal representation and there was no excessive time required to sum 50 to 100 terms of a Fourier-series approximation to the input and outputs.

---

* Work of Stenton and collaborators, as yet unpublished.

b.) Intersecting Surfaces

In connection with adapting interference theory to intersecting surfaces, an exhaustive study has been carried out on exact linearized solutions in steady flow. Some of the configurations analyzed are sketched in Fig. 16. Included have been general cruciform combinations according to slender-body theory, cruciform supersonic delta combinations with subsonic and supersonic leading edges according to conical flow theory, and slender-body representations of V and T-tails, etc. In all cases, no singular behavior is found near any corner where the surfaces meet at an angle less than or equal to 180°. Indeed, one can speculate on a general conclusion that seems reasonable physically: regardless of flight Mach number, the crossflow in the corner behaves like the familiar, two-dimensional, incompressible corner-flow solution

$$\varphi = K r^{\frac{\pi}{\delta}} \cos\frac{\pi\theta}{\delta} \quad , \tag{54}$$

δ being the angle and r, θ polar coordinates at the corner.

The v and w velocity components are proportional to the power ($\frac{\pi}{\delta}$ -1) of r, reducing to linear dependence in a rectangular corner. The three-dimensional disturbance pressure has an extreme value at the corner and varies only slowly in the vicinity. Hence there would seem to be no problem constructing suitable pressure series, generalizing Eq. (18), when analyzing such intersections, except at the outer side of a V-tail.

c.) The Question of Nonlinearity

The relatively thick lifting surfaces of some entry vehicles, the push to higher cruising Mach numbers, and the appearance of heavily-loaded aircraft for flight near the ground are among the many reasons why the small-disturbance restriction on aerodynamic theory is often intolerable. Nevertheless, linearized methods like those described in this paper are already so complicated as to inspire pessimism regarding refinements. It is unwise to speculate too extensively about incomplete developments, but it should be pointed out that certain routes exist by which nonlinearity can be introduced, both for planar wings and interacting surfaces.

b.) Intersecting Surfaces

In connection with adapting interference theory to intersecting surfaces, an exhaustive study has been carried out on exact linearized solutions in steady flow. Some of the configurations analyzed are sketched in Fig. 16. Included have been general cruciform combinations according to slender-body theory, cruciform supersonic delta combinations with subsonic and supersonic leading edges according to conical flow theory, and slender-body representations of V and T-tails, etc. In all cases, no singular behavior is found near any corner where the surfaces meet at an angle less than or equal to 180°. Indeed, one can speculate on a general conclusion that seems reasonable physically: regardless of flight Mach number, the crossflow in the corner behaves like the familiar, two-dimensional, incompressible corner-flow solution

$$\varphi = K r^{\frac{\pi}{\delta}} \cos\frac{\pi\theta}{\delta} \quad , \tag{54}$$

δ being the angle and r, θ polar coordinates at the corner.

The v and w velocity components are proportional to the power $(\frac{\pi}{\delta} - 1)$ of r, reducing to linear dependence in a rectangular corner. The three-dimensional disturbance pressure has an extreme value at the corner and varies only slowly in the vicinity. Hence there would seem to be no problem constructing suitable pressure series, generalizing Eq. (18), when analyzing such intersections, except at the outer side of a V-tail.

c.) The Question of Nonlinearity

The relatively thick lifting surfaces of some entry vehicles, the push to higher cruising Mach numbers, and the appearance of heavily-loaded aircraft for flight near the ground are among the many reasons why the small-disturbance restriction on aerodynamic theory is often intolerable. Nevertheless, linearized methods like those described in this paper are already so complicated as to inspire pessimism regarding refinements. It is unwise to speculate too extensively about incomplete developments, but it should be pointed out that certain routes exist by which nonlinearity can be introduced, both for planar wings and interacting surfaces.

Consider, for instance, the ideas of Covert (Ref. 30) and others regarding steady motion of supersonic wings. Reference 30 demonstrates that second-order effects of thickness in the near field are properly accounted for if the disturbance potential Φ of the lifting flow is made to satisfy the differential equation

$$(M_T^2 - 1)\Phi_{xx} - \Phi_{yy} - \Phi_{zz} + \lambda \Phi_x = 0 \tag{55}$$

where M_T is the local surface Mach number due to the thickness distribution and λ is often a very small parameter. Covert shows how Φ can be then built up by superposition of source-like solutions depending on M_T rather than free-stream M. Thus one corrects for variations in sound speed and second-order convection effects, while still ignoring shocks which are third-order.

There is no evident reason why Covert's scheme cannot be adapted to nonplanar surfaces and to lifting flows which are simple harmonic rather than steady. An attempt to mechanize his results for digital computation could constitute a fruitful undertaking.

Already referred to above was the suggestion of Landahl (Ref. 28) for a refinement on linearized, transonic theory that parallels Covert's development very closely. Landahl focusses on simple harmonic motion and again demonstrates how the unsteady perturbation potential can be found from a differential equation whose coefficients depend on the local sonic and particle speeds in the thickness flow. It might be observed that, for numerical computation, there is no reason why steady data to be incorporated in such theories cannot be obtained experimentally.

For finite wings oscillating at subsonic Mach numbers, the author is aware of no mathematically consistent nonlinear analyses. This lack does not, however, preclude an attempt to make semi-empirical corrections for thickness and interference that might extend the methods of this paper to more heavily-loaded systems. The key idea is that proposed for two-dimensional airfoils by Allen (Ref. 31). Once the aggregation of vortices or acceleration-potential doublets representing the lifting flow is determined

by linearized procedures, one can compute the local streamwise velocity ($U + \varphi_x$) at each such element. The load would then be estimated by replacing U with ($U + \varphi_x$) in Bernoulli's equation or the Kutta-Joukowsky theorem. This has produced significant improvements in a number of steady cases and merits further examination in connection with the interference problem.

d.) Conclusions

When concluding, it seems necessary to point out only that a pattern is emerging in the treatment of three-dimensional loading of wings and interacting systems by means of linearized aerodynamic theory. A host of questionably consistent approximations are being replaced by the systematic superposition of appropriate singularities which, in the limit of an infinite number of terms, would produce an exact solution. The unifying tool is the high-speed digital computer.

Illustrative calculations have been presented or referenced for subsonic, sonic and supersonic flight Mach numbers, involving both steady and oscillatory motion. The number and variety of these is deemed sufficient to portend the widespread development of these methods and their forthcoming availability as another string for the aircraft designer's bow.

VII. References

1. Ferrari, C., Interaction Problems, Section C, Vol. VII, of High Speed Aerodynamics and Jet Propulsion, Princeton University Press, Princeton, New Jersey, 1957.

2. Lawrence, H. R., and Flax, A. H., Wing-Body Interference at Subsonic and Supersonic Speeds-Survey and New Developments, Journal of the Aeronautical Sciences, Vol. 21, No. 5, May 1954, pp. 289-328.

3. Ward, G. N., Linearized Theory of High Speed Flow, Cambridge University Press, 1955.

4. Bryson, A. E., Stability Derivatives for a Slender Missile with Application to a Wing-Body-Vertical-Tail Configuration, Journal of the Aeronautical Sciences, Vol. 20, No. 5, May 1953, pp. 297-308.

5. Spreiter, J. R., The Aerodynamic Forces on Slender Plane—and Cruciform—Wing and Body Combinations, N. A. C. A. Report 962, 1950.

6. Adams, M. C., and Sears, W. R., Slender Body Theory—Review and Extension, Journal of the Aeronautical Sciences, Vol. 20, No. 2, February 1953, pp. 85-98.

7. Miles, J. W., The Potential Theory of Unsteady Supersonic Flow, Cambridge University Press, 1959.

8. Ashley, H., Zartarian, G., and Neilson, D. O., Investigation of Certain Unsteady Aerodynamic Effects in Longitudinal Dynamic Stability, U. S. A. F. Technical Report 5986, 1951.

9. Statler, I. C., Derivation of Dynamic Longitudinal Stability Derivatives for Subsonic Compressible Flow from Nonstationary Flow Theory and Application to an F-80A Airplane, Cornell Aeronautical Laboratory Report No. TB-495-F-9, 1949.

10. Statler, I. C., and Easterbrook, M., Handbook for Computing Nonstationary Flow Effects on Subsonic Dynamic Longitudinal Response Characteristics of an Airplane, Cornell Aeronautical Laboratory Report No. TB-495-F-12, 1950.

11. Landahl, M. T., Unsteady Transonic Flow, Pergamon Press, New York-Oxford-London-Paris, 1961.

12. Zartarian, G., et al., Forces and Moments on Oscillating Slender Wing-Body Combinations at Supersonic Speed, Parts I and II, U. S. Air Force Office of Scientific Research Technical Notes 57-386 and 58-114, 1957.

13. Mangler, K. W., Improper Integrals in Theoretical Aerodynamics, British Royal Aircraft Establishment, Report No. Aero 2424.

14. Watkins, C. E., Runyan, H. L., and Woolston, D. S., On the Kernel Function of the Integral Equation Relating the Lift and Downwash Distributions of Oscillating Finite Wings at Subsonic Speeds, N. A. C. A. Report 1234, 1955.

15. Watkins, C. E., Woolston, D. S., and Cunningham, H. J., A Systematic Kernel Function Procedure for Determining Aerodynamic Forces on Oscillating or Steady Finite Wings at Subsonic Speeds, N. A. S. A. Report R-48, 1959.

16. Hsu, P. T., Some Recent Developments in Flutter Analysis of Low-Aspect-Ratio Wings, Proceedings of the National Specialists Meeting on Dynamics and Aeroelasticity, Ft. Worth, Texas, Nov., 1958, published by Institute of the Aeronautical Sciences, pp. 7-26.

17. Stark, V. J. E., Aerodynamic Forces on Rectangular Wings Oscillating in Subsonic Flow, Saab Technical Note 44, Saab Aircraft Company, Sweden, 1960.

18. Cunningham, H. J., and Woolston, D. S., Developments in the Flutter Analysis of General Plan Form Wings Using Unsteady Air Forces from the Kernel Function Procedure, Proceedings of the National Specialists Meeting on Dynamics and Aeroelasticity, Ft. Worth, Texas, Nov. 1958, pp. 27-36.

19. Saunders, G. H., Aerodynamic Characteristics of Wings in Ground Proximity, Master of Science Thesis, Massachusetts Institute of Technology, June 1963.

20. Landahl, M. T., Ashley, H., and Widnall, S. M., Some Free Surface Effects on Unsteady Hydrodynamic Loads and Hydroelasticity, Proceedings of the Fourth Symposium on Naval Hydrodynamics, Washington, D. C., August 1962, Office of Naval Research ACR-73, pp. 490-518.

21. Crimi, P., and Statler, I. C., Forces and Moments on an Oscillating Hydrofoil, Proceedings of the Fourth Symposium on Naval Hydrodynamics, op. cit., pp. 447-466.

22. Smith, A. M. O., and Pierce, J., Exact Solution of the Neumann Problem. Calculation of Non-Circulatory Plane and Axially Symmetric Flows about or within Arbitrary Boundaries, Douglas Aircraft Company Report No. ES26988, April 1958.

23. Pines, S., Dugundji, J., and Neuringer, J., Aerodynamic Flutter Derivatives for a Flexible Wing with Supersonic and Subsonic Edges, Journal of the Aeronautical Sciences, Vol. 22, No. 10, October 1955, pp. 693-700.

24. Zartarian, G., and Hsu, P. T., Theoretical Studies on the Prediction of Unsteady Supersonic Airloads on Elastic Wings, Parts I and II, U. S. Air Force, Wright Air Development Center. Technical Report 56-97, Part I, Dec. 1955, Part II, Feb. 1956.

25. Watkins, C. E., Effect of Aspect Ratio on the Air Forces and Moments of Harmonically Oscillating Thin Rectangular Wings in Supersonic Potential Flow, N. A. C. A. Report 1028, 1951.

26. Ashley, H., Supersonic Airloads on Interfering Lifting Surfaces by Aerodynamic Influence Coefficient Theory, The Boeing Company Report No. D2-22067, November 1962.

27. Rodden, W. P., and Revell, J. D., The Status of Unsteady Aerodynamic Influence Coefficients, S. M. F. Fund Paper No. FF-33, presented at Annual Meeting, Institute of the Aerospace Sciences, January 1962.

28. Landahl, M. T., Linearized Theory for Unsteady Transonic Flow, paper presented at Symposium Transsonicum, Aachen, Germany, September 1962 (also Issued as MIT Fluid Dynamics Research Laboratory Report No. 63-2, March 1963).

29. Bisplinghoff, R. L., et al., An Investigation of Stresses in Aircraft Structures under Dynamic Loading, Massachusetts Institute of Technology, Aeroelastic and Structures Research Laboratory Report for U. S. Navy Bureau of Aeronautics, January 1949.

30. Covert, E. E., The Aerodynamics of Distorted Surfaces, Proceedings of the Symposium on Aerothermoelasticity, U. S. Air Force Aeronautical Systems Division Technical Report 61-645, October 1961, pp. 369-406.

31. Allen, H. J., General Theory of Airfoil Sections Having Arbitrary Shape or Pressure Distribution, N. A. C. A. Report 833, 1945.

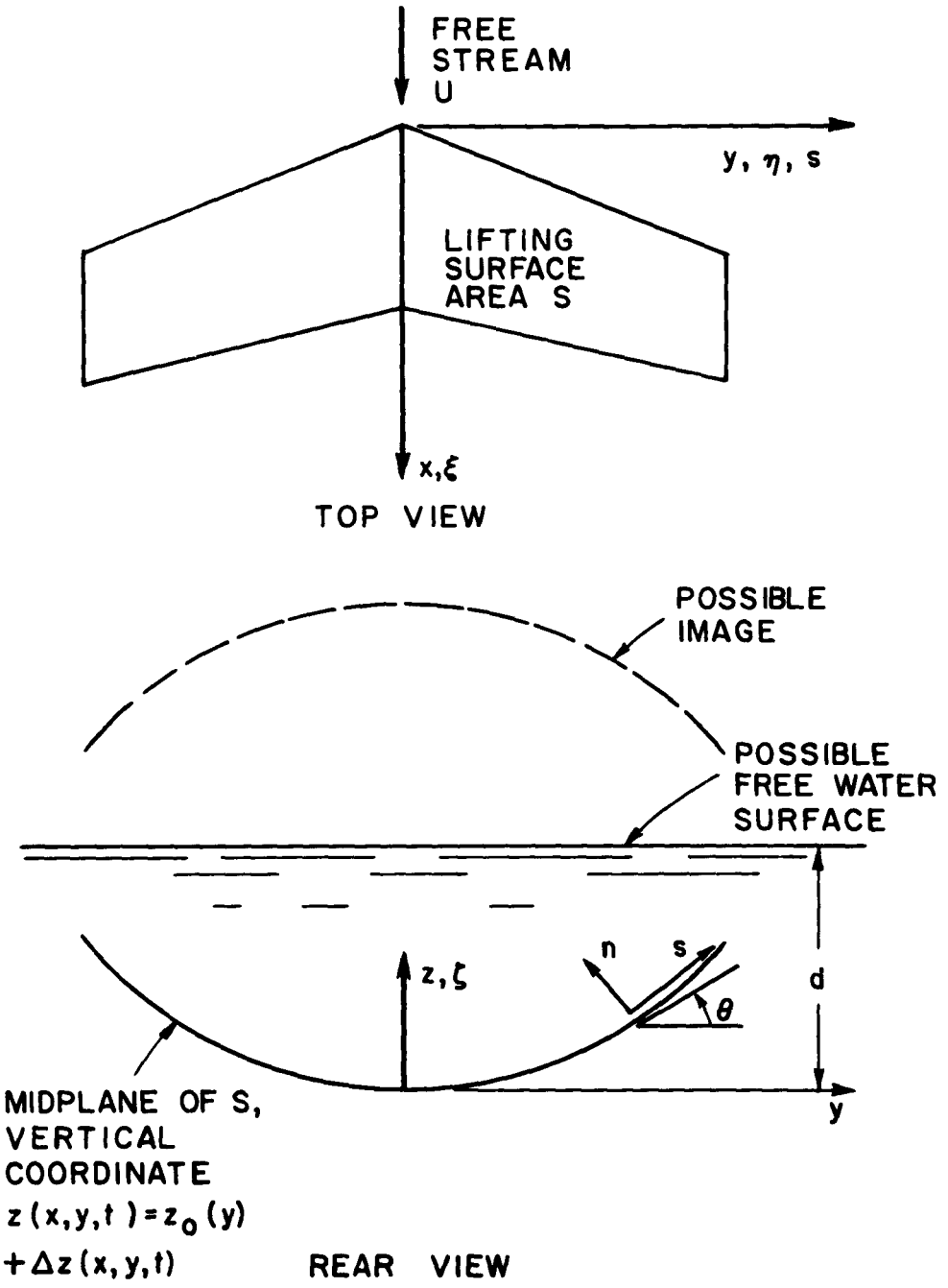

Fig. 1 - Top and rear elevations of a thin, nonplanar lifting surface performing small unsteady motions normal to a uniform subsonic or supersonic stream flowing parallel to the x-coordinate. The image of this wing in a ground plane or free water surface is shown.

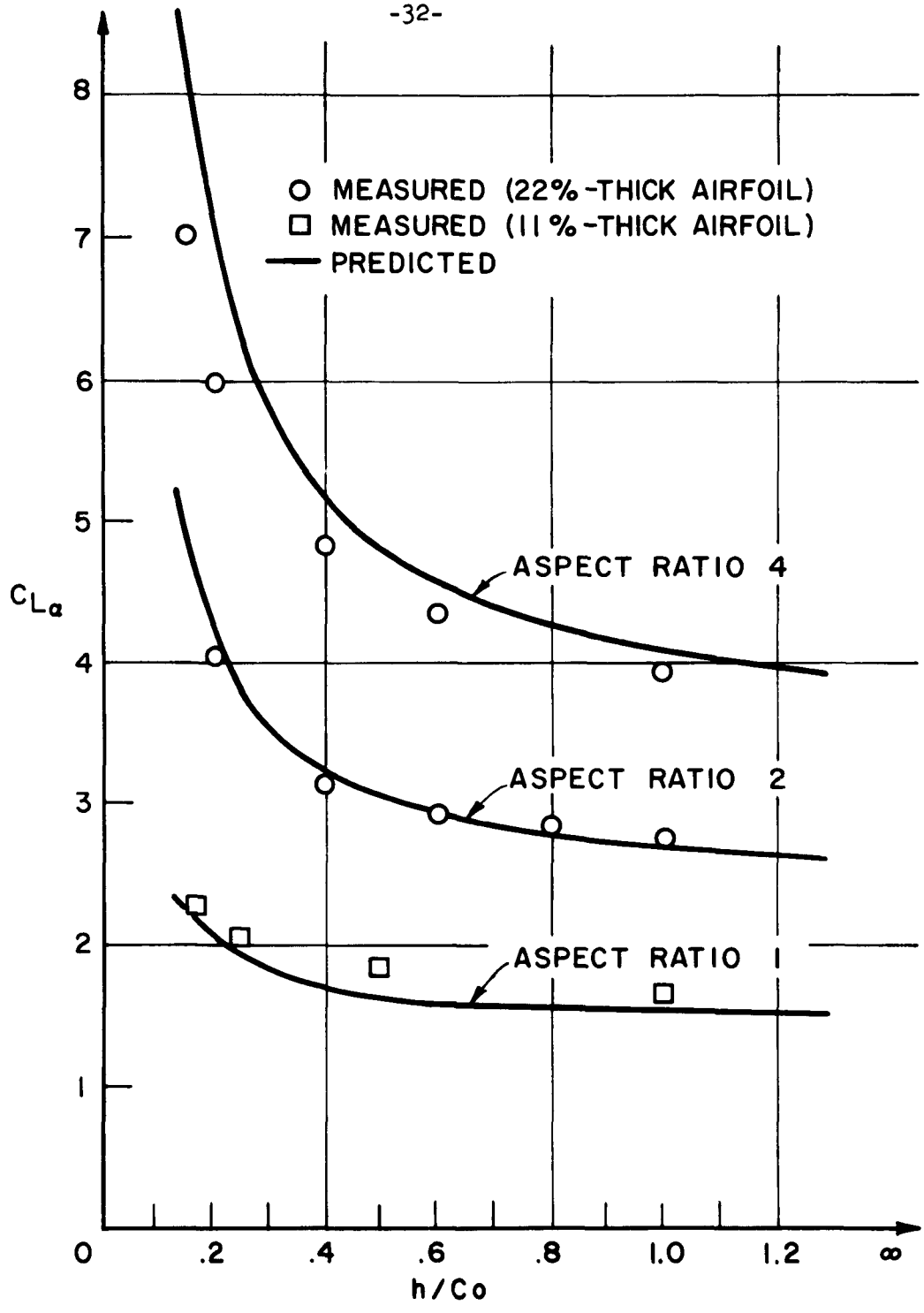

Fig. 2 - Steady lift-curve slopes of three rectangular, plane wings as functions of distance above a ground plane measured in wing chords. (Figures 2-7 refer to constant density fluid.)

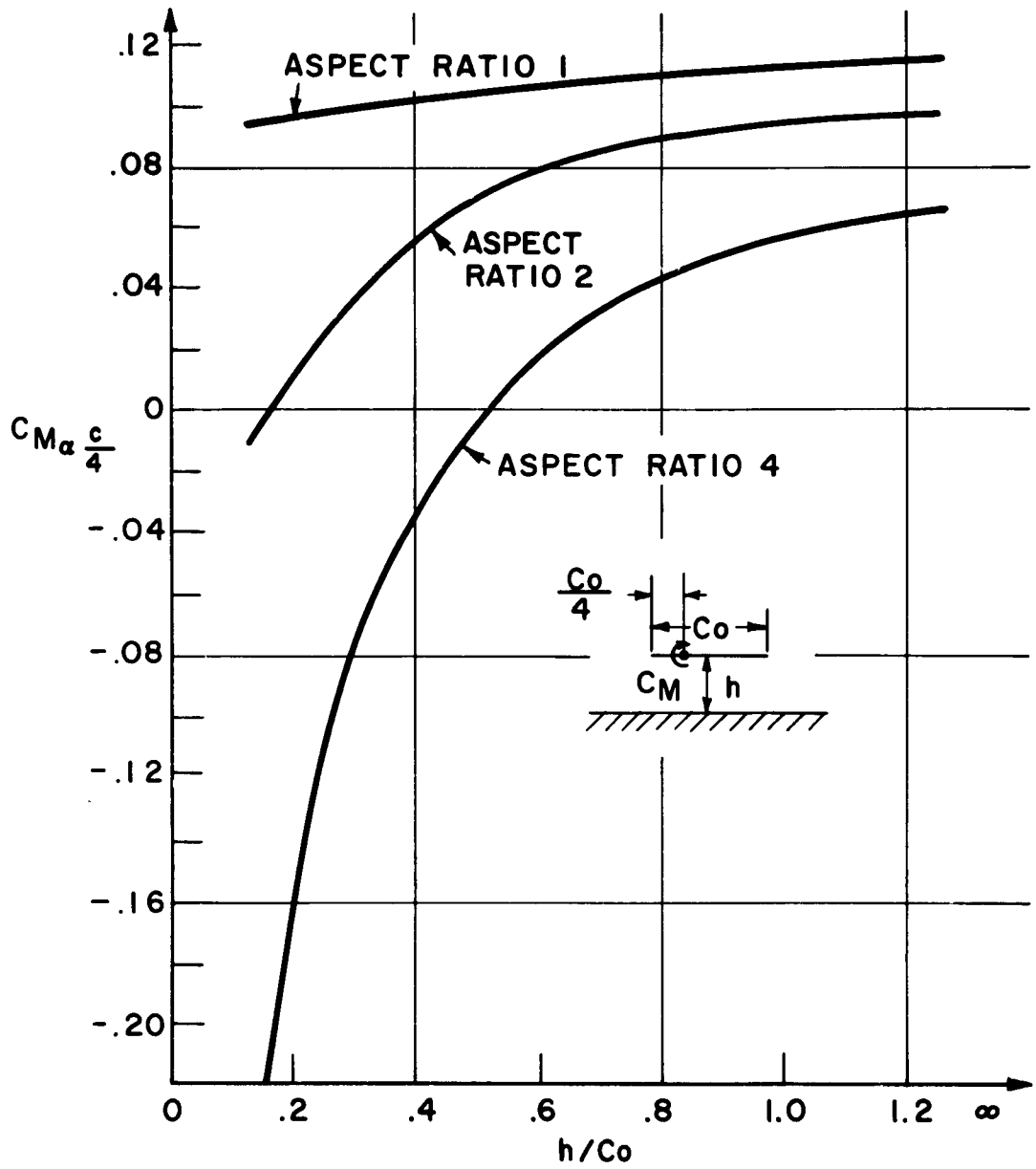

Fig. 3 - Curves of nose-up pitching moment coefficient, taken per unit angle of attack about an axis along the quarter-chord line, for three rectangular wings. Abscissa is distance above a ground plane measured in chords.

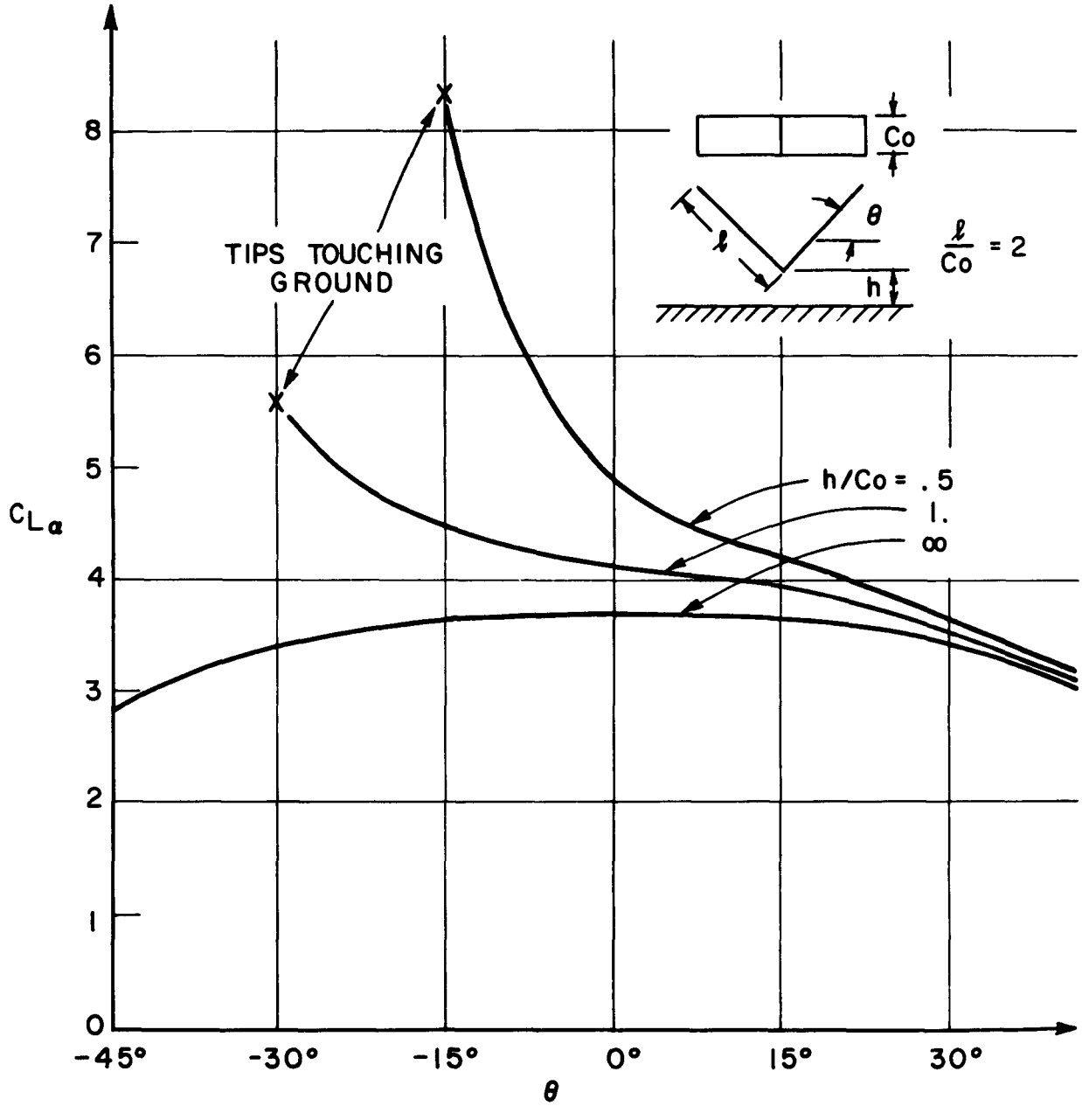

Fig. 4 - Steady lift-curve slope vs. dihedral angle, for the illustrated V-wing at three different centerline heights h above a ground plane.

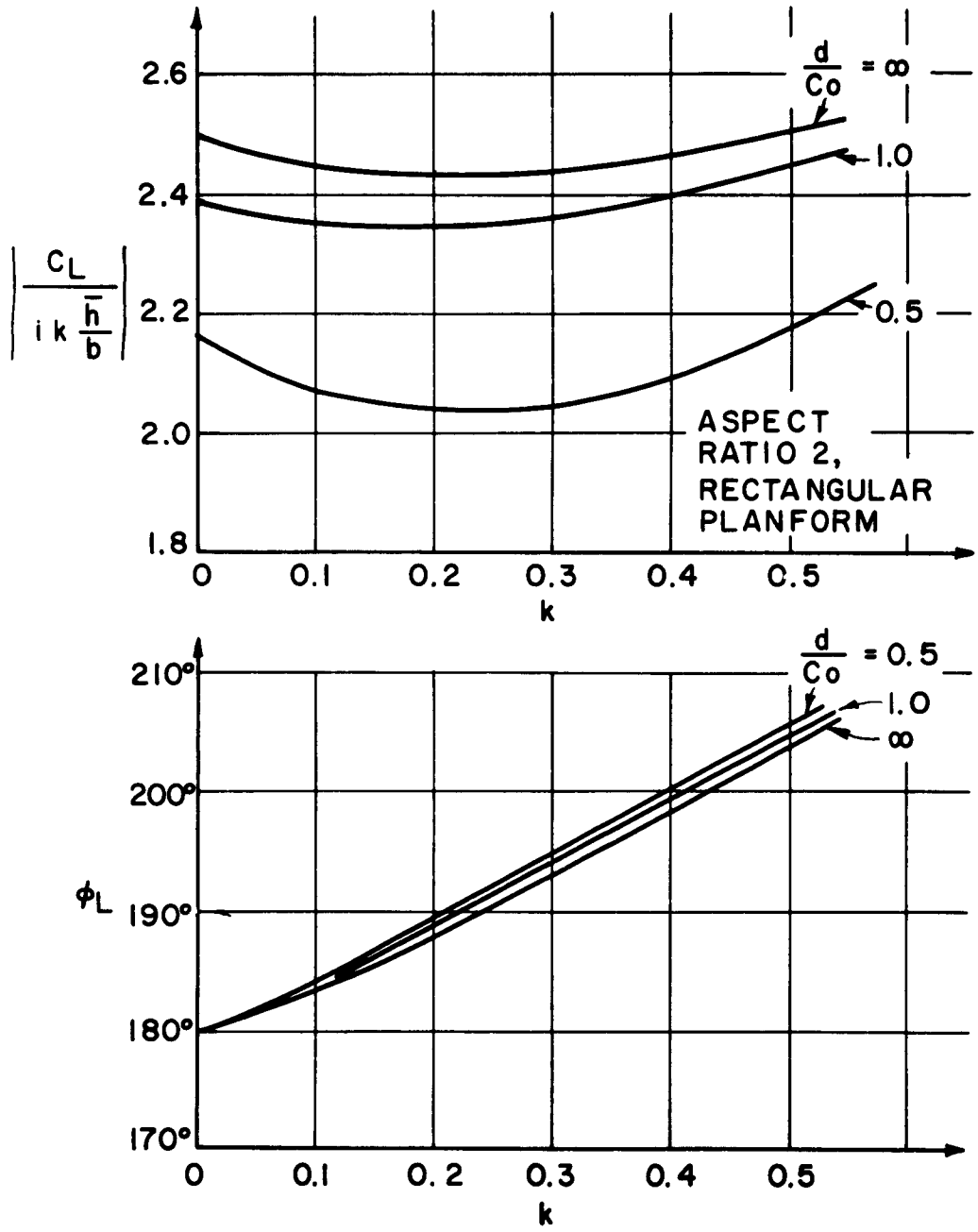

Fig. 5 - Magnitude and phase angle of dimensionless lift due to vertical-translation oscillation of a rectangular hydrofoil, plotted vs. reduced frequency $k = \omega b/U$. Three depths below a free water surface at high Froude number are indicated.

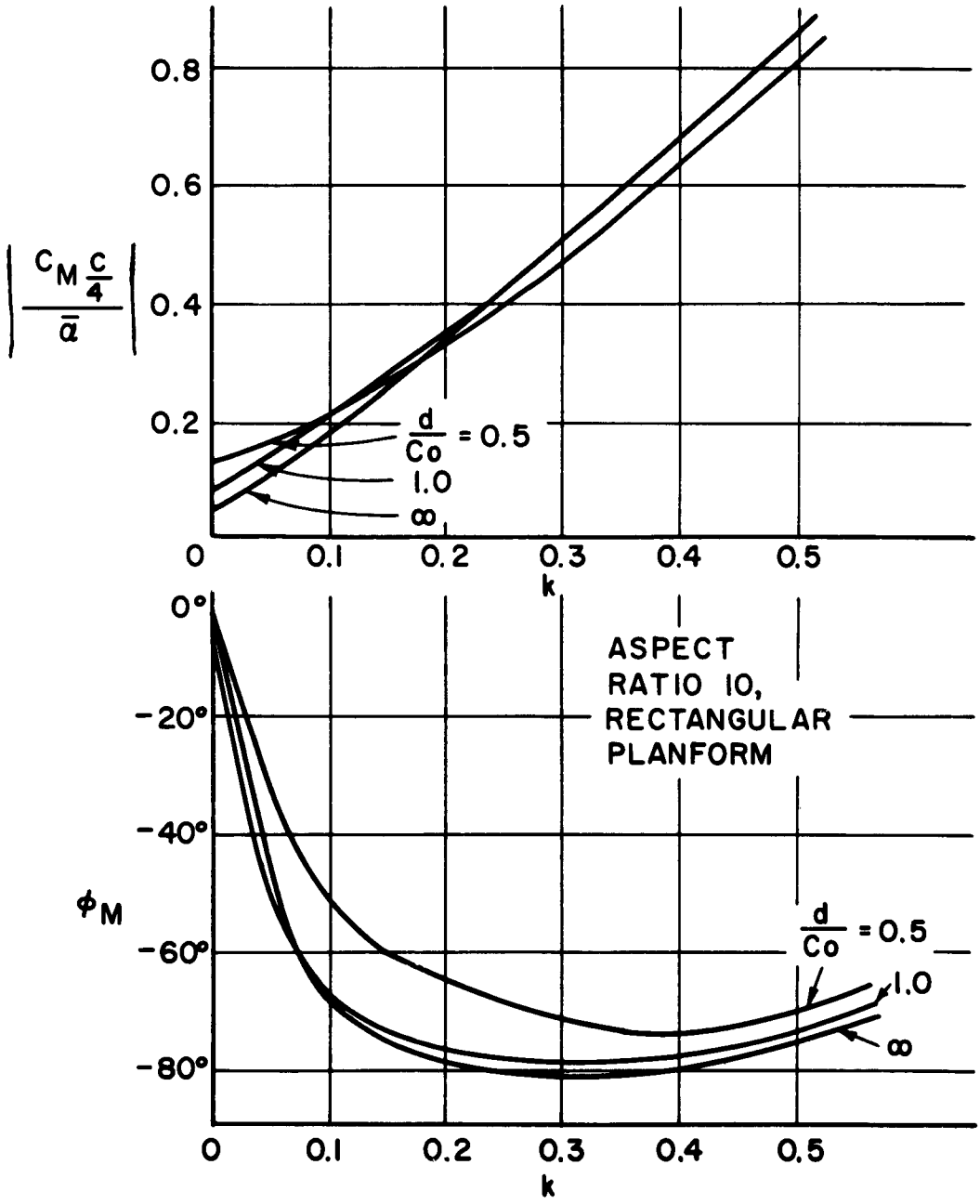

Fig. 6 - Magnitude and phase angle of dimensionless quarter-chord pitching moment due to pitching oscillation about the moment axis by a rectangular hydrofoil. Abscissa is reduced frequency. Three depths below a free water surface at high Froude number are indicated.

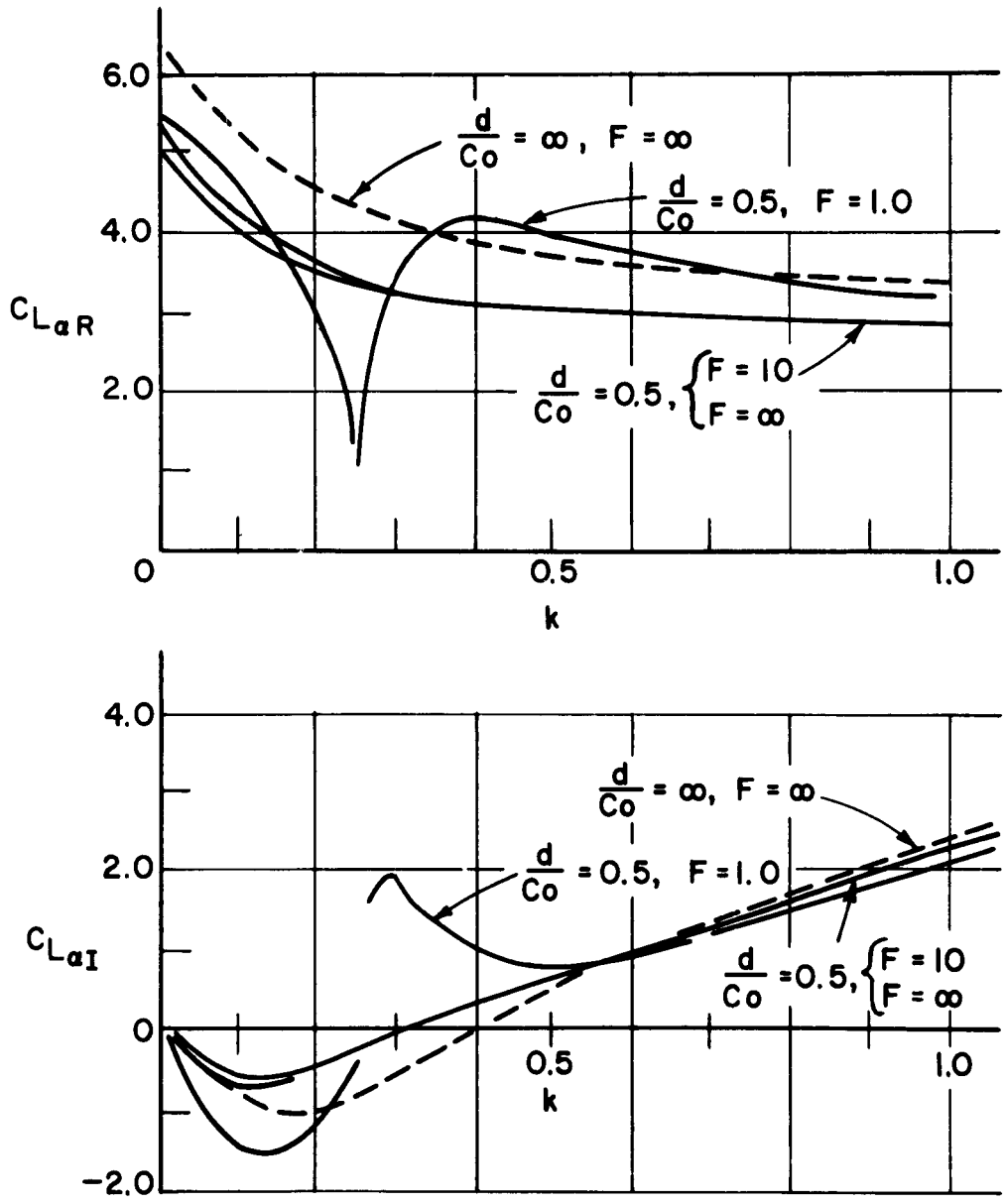

Fig. 7 - Real and imaginary parts of dimensionless lift due to pitching oscillation of a two-dimensional hydrofoil running parallel to a free surface. Four combinations of depth-to-chord ratio and Froude number are shown. Infinite depth case corresponds to classical oscillating airfoil theory for incompressible flow.

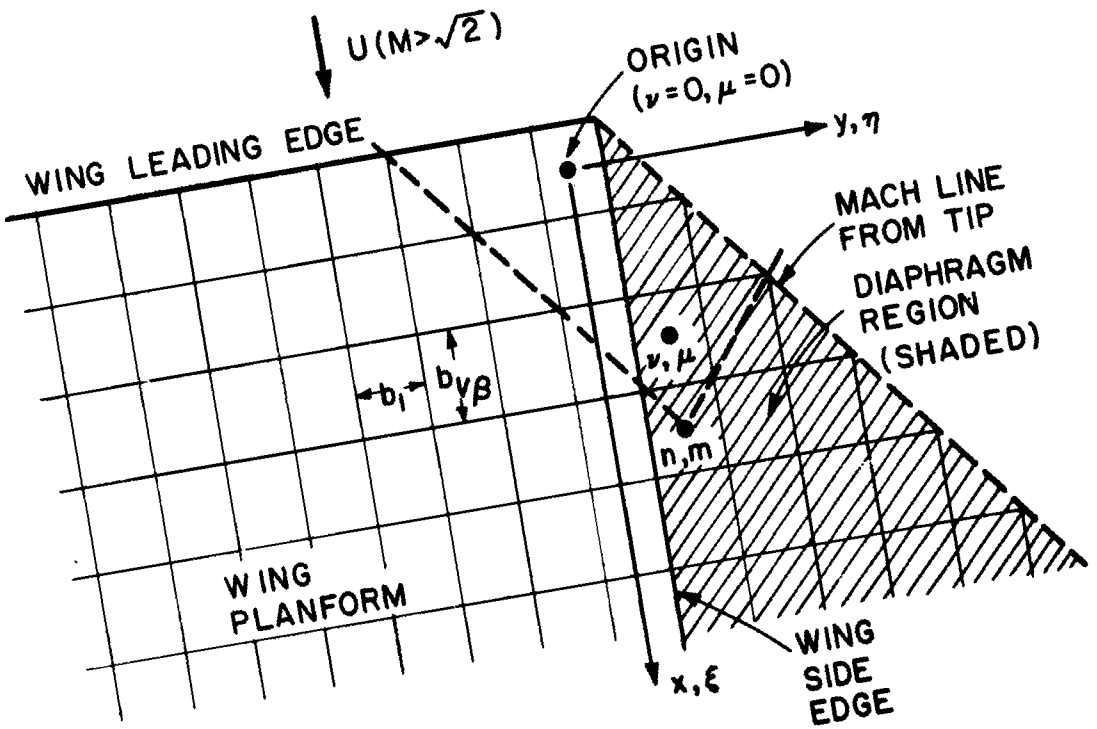

Fig. 8 - Illustrating right wingtip region of a plane, rectangular wing in supersonic flow overlaid with elementary rectangular areas having diagonals parallel to the Mach lines. (ν, μ) and (n, m), respectively, are pairs of integers identifying chordwise and spanwise centers of areas that "send" and "receive" signals.

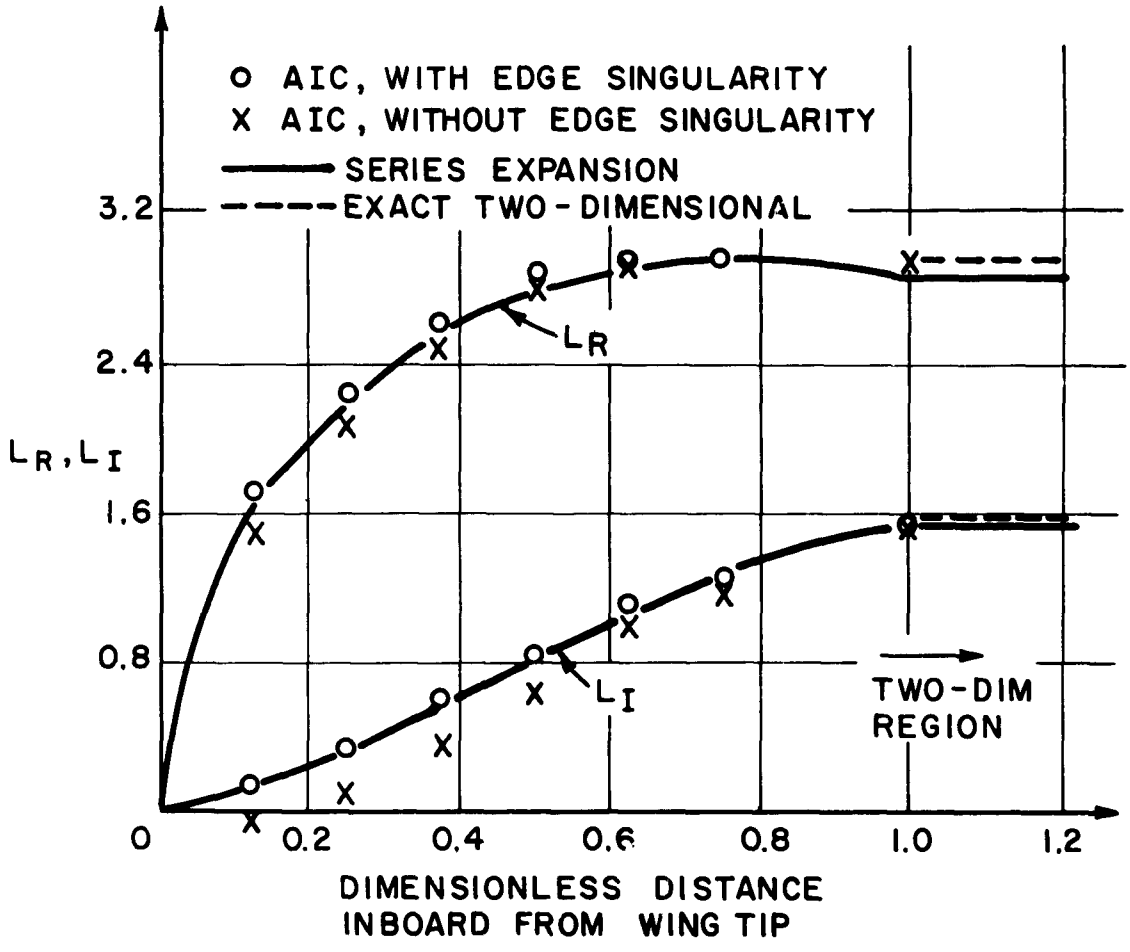

Fig. 9 - Four theoretical calculations of the dimensionless lift per unit span in the wingtip region of a plane, rectangular wing in vertical-translation oscillation normal to a supersonic stream at $M=1.2$. Reduced frequency based on semichord is $k=1.3$. AIC refers to method of velocity potential aerodynamic influence coefficients with four area elements along the chord.

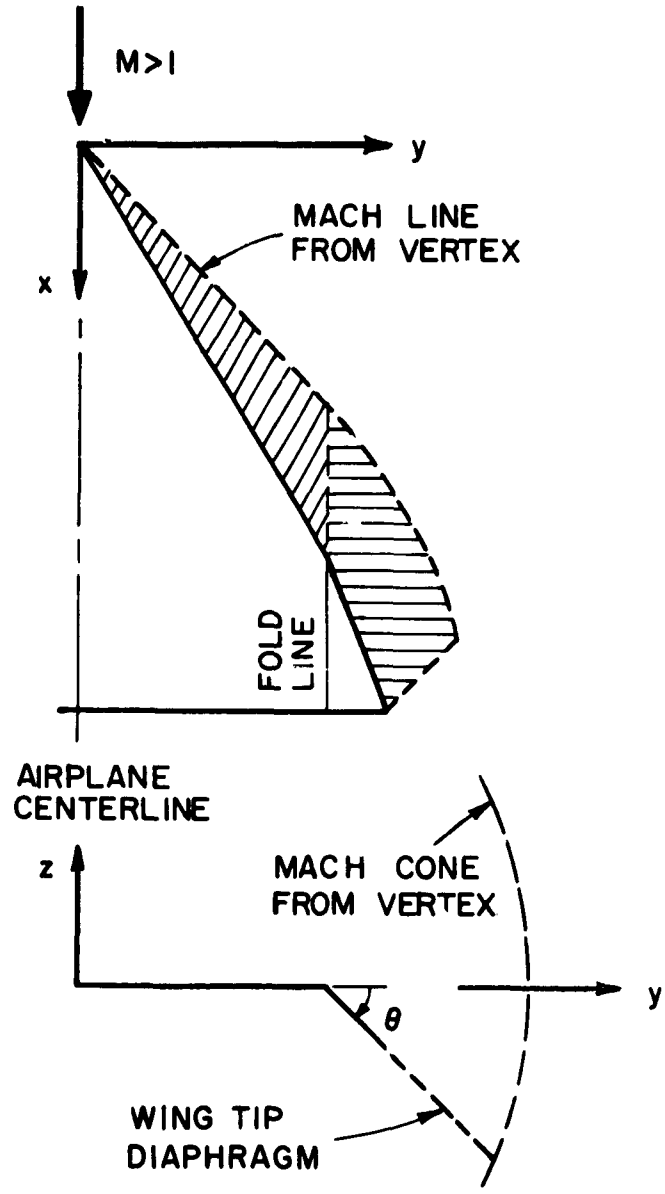

Fig. 10 - Top and rear elevations of a triangular wing in supersonic flow with wingtip folded downward. Shown shaded is a suitable diaphragm area for isolating the upper and lower surfaces.

(Figure 11 has not yet
been released for publication.)

Fig. 11

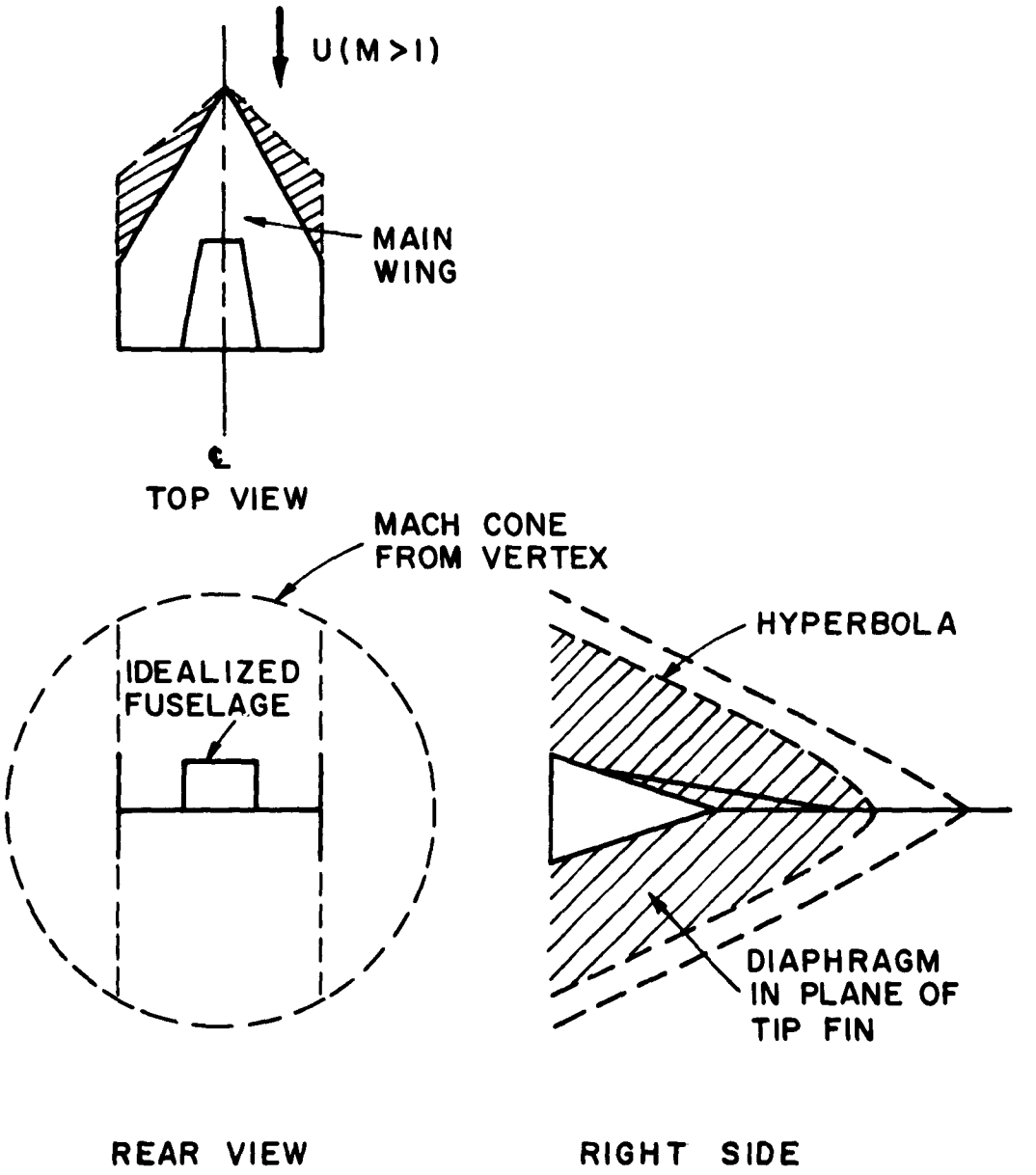

Fig. 12 - Typical configuration of a hypersonic glider flying at low supersonic speed, with suitable diaphragm areas for isolating the opposite sides of each lifting surface. Diaphragms are shown shaded.

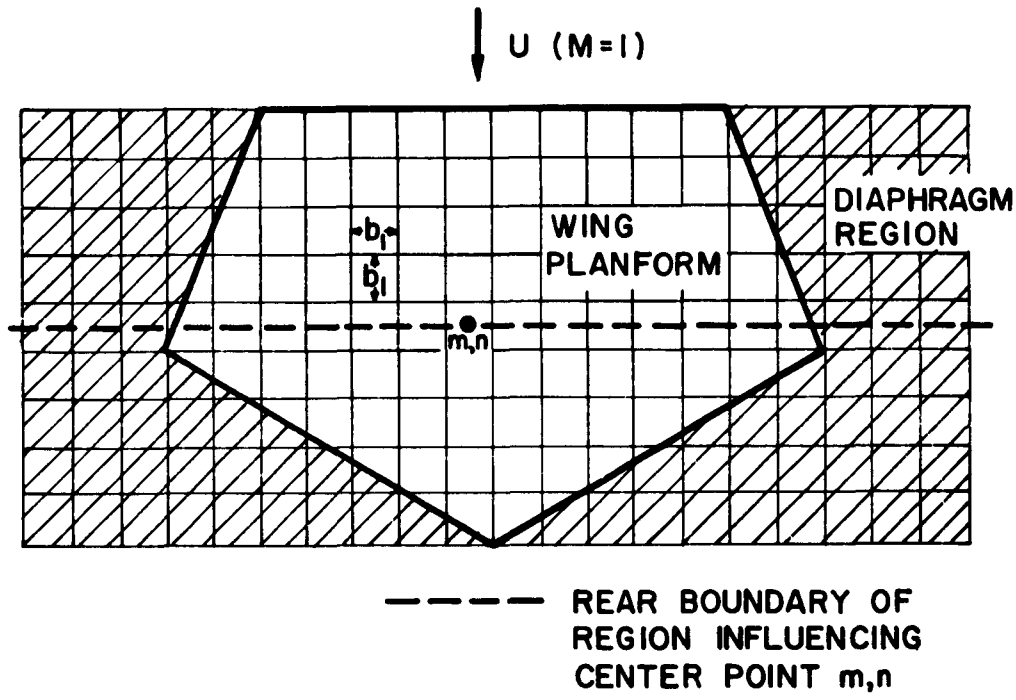

Fig. 13 - A plane wing flying at sonic speed. Illustrated is a pattern of square area elements suitable for application of oscillatory aerodynamic influence coefficients. Under strictly linearized theory, all areas ahead of the spanwise dashed line can affect the central point identified by the integers m,n.

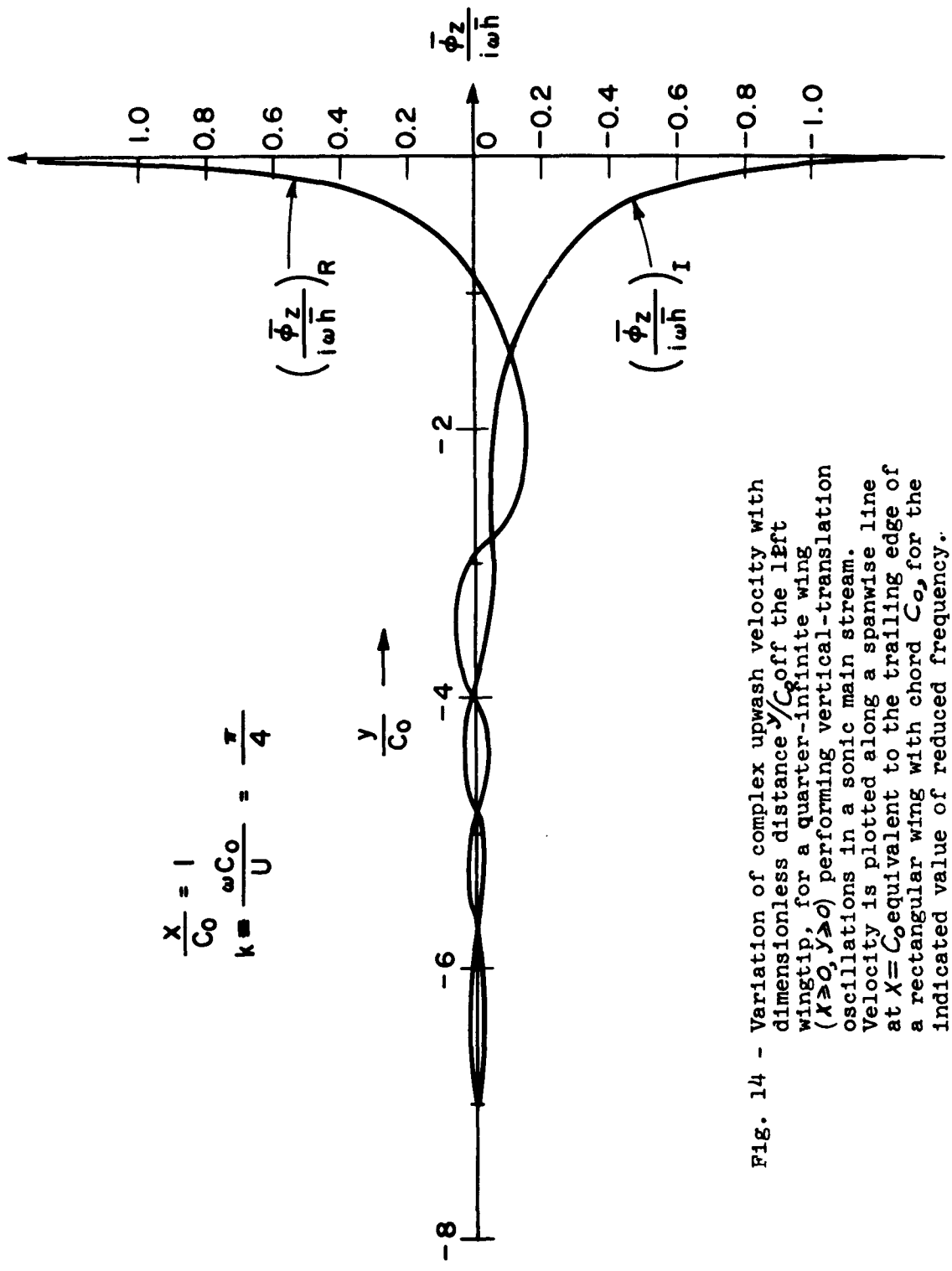

Fig. 14 - Variation of complex upwash velocity with dimensionless distance y/C_0 off the left wingtip, for a quarter-infinite wing ($x \geq 0, y \geq 0$) performing vertical-translation oscillations in a sonic main stream. Velocity is plotted along a spanwise line at $x = C_0$ equivalent to the trailing edge of a rectangular wing with chord C_0, for the indicated value of reduced frequency.

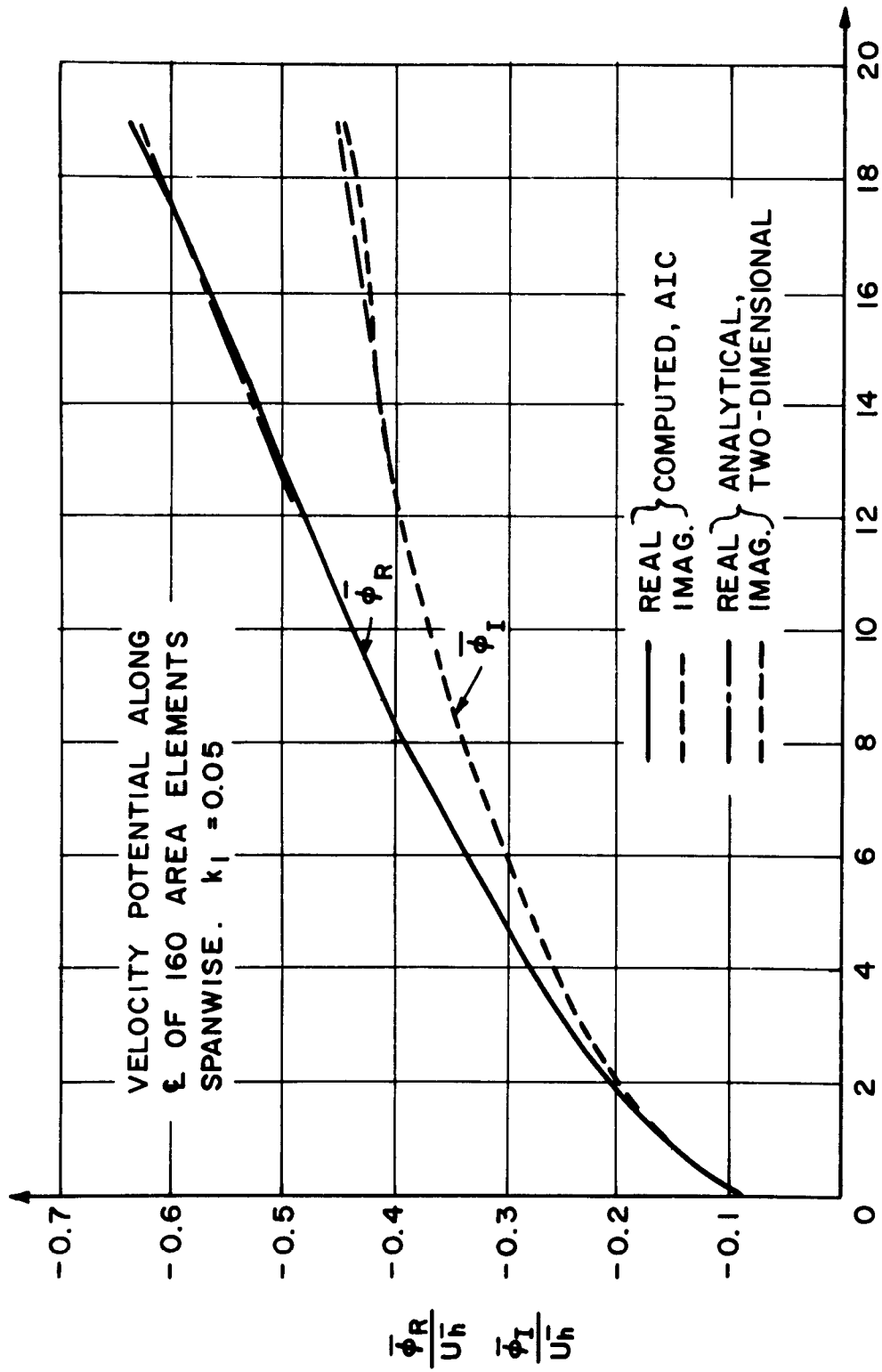

Fig. 15 - Dimensionless complex velocity potential as a function of chordwise position on upper surface of a wing in vertical-translational oscillation in a sonic main stream. Exact two-dimensional results are compared with aerodynamic-influence-coefficient calculation with 80 area elements spanwise on either side of the station. Reduced frequency based on area-element dimension is 0.05.

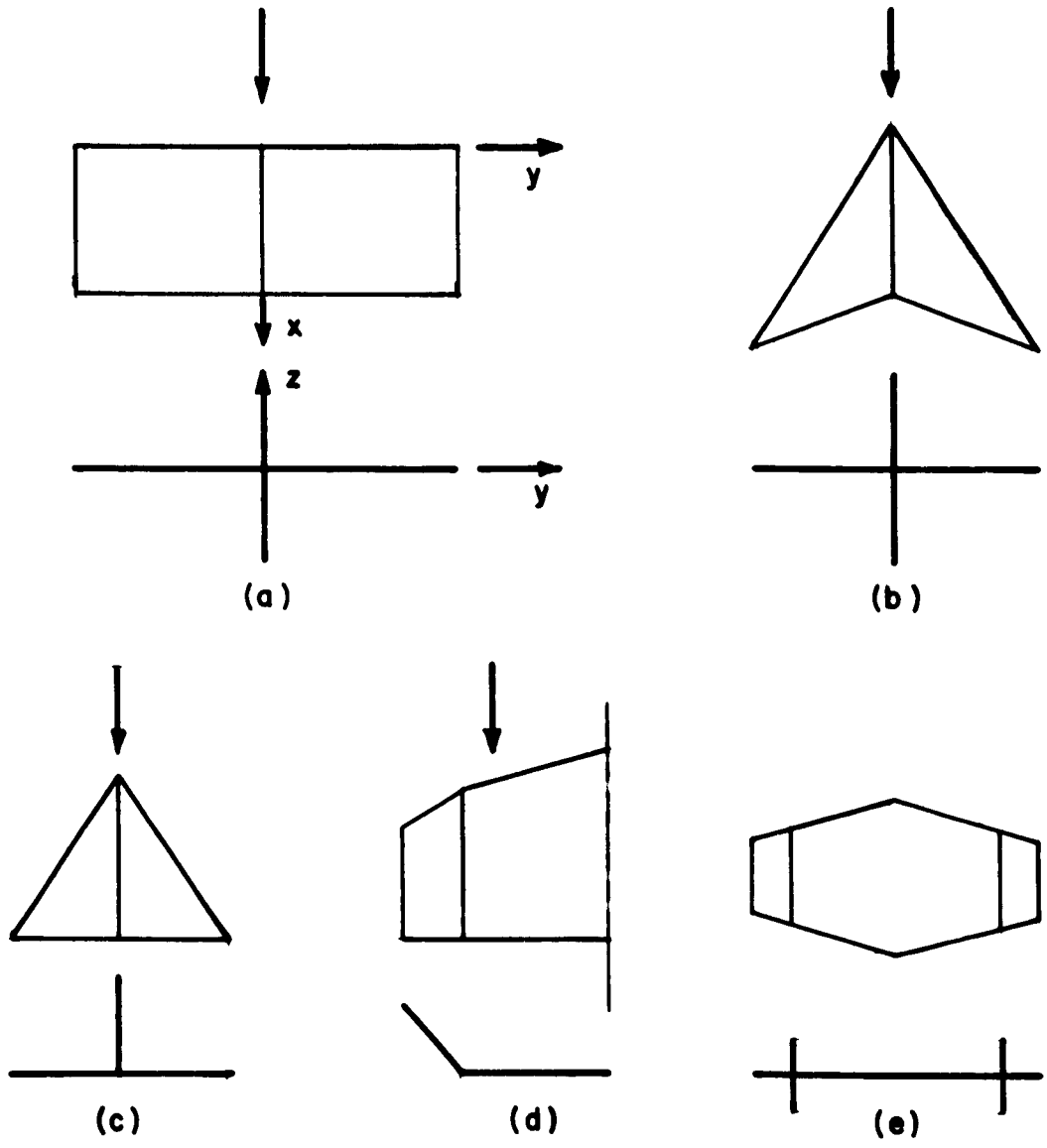

Fig. 16 - Top and rear views of various intersecting configurations whose loading can be determined by numerical methods of this paper. Several simple cases like these have been analyzed in closed form for comparison purposes.